# Lithological and Geomorphological Indicators of Glacial Genesis in the Upper Quaternary Strata, Nadym River Basin

Oleg Sizov[1], Anna Volvakh[2], Molodkov A.N.[3], Andrey Vishnevskiy[4], Andrey Soromotin[5], and Evgeny Abakumov[6]

[1]Oil and Gas Research Institute, Russian Academy of Sciences, Moscow, Russia
[2]Sobolev Institute of Geology and Mineralogy, Siberian Branch of Russian Academy of Sciences, Novosibirsk, Russia
[3]Tallin Technological University, Tallin, Estonia
[4]Novosibirsk State University, Novosibirsk, Russia
[5]Tyumen State University, Tyumen, Russia
[6]Saint-Petersburg State University, Saint Petersburg, Russia

## Abstract

Analyzing the genesis of Quaternary sediments is important for understanding the glaciation history and development of marine sediments in the northern part of Western Siberia. The problem is relevant since there is no consistent concept of the Quaternary sediments genesis in the north of Western Siberia. Their formation is associated with marine, glacial and interglacial sedimentation conditions. The research objective is to identify the persistent features characterizing the conditions of sedimentation and relief formation using the Nadym river basin as an example. The best method for studying this problem is a comprehensive analysis of the lithological, chronostratigraphic, petrographic and geomorphological studies of the Quaternary sediments upper strata. This study provides data from the analysis of the basic characteristics of quartz grains at the site. The rounding and morphology of the quartz grains provide evidence of possible glacial processing of some of the site strata. A petrographic study of selected boulder samples was performed. Some of them, by the shape and presence of striation, can be attributed to glacial basins. The first use of a detailed digital elevation model applied to the study area made it possible to identify specific relief forms that could very likely be created during glaciations. Based on the analysis, we propose to consider the vast lake-alluvial plains in the Nadym river basin as periglacial regions. This idea lays the lithological framework for understanding the reasons for the formation of the modern landscape structure. The materials and descriptions provided are of interest to researchers of Quaternary sediments, topography, vegetation, and soil cover; particularly researchers engaged in revising the history of the natural environment development in the north of Western Siberia.

*Keywords: Western Siberia, paleogeography, cover glaciation, Quaternary deposits, quartz grains, petrography, DEM*

### *Introduction*

The history of geomorphological development in the northern part of Western Siberia was a subject of intensive discussion at the end of the 20th century. The stratigraphy of the Yenisey and Ob estuary is a key factor of the West-Siberian lowland Quaternary evolution. Numerous examples of sedimentation alternation induced by various cover glaciations of different ages and thicknesses are presented. This series of sediments was used as a background for geological interpretation of the history of West-Siberian lowland. The Q-43 national geological map of Russia for this region indicates the dominance of glacial and fluvioglacial types of the surface sediments (Alyavdin and Mokin, 1957). The possible existence of ice sheets and related permafrost sediments was identified as a key issue at the beginning of

the systematic geological study of the north of West Siberia in the 1960s. Some researchers (e.g., Svendsen et al., 2004) suggested that there were extensive glaciations that resulted in blocking the Ob, Yenisei, Pur, Taz, Nadym rivers at certain stages, leading to the formation of large glacier dammed lakes (Grosvald, 1999).

Another point of view considers possible glaciation on the plain (e.g., Generalov, 1986). It explains why the landforms are a sequence of terraces formed by marine transgressions of various ages. There is also an opinion that the glaciation was localized in the form of ice caps on separate watersheds and that the river flows of the Ob, Yenisei, and other rivers were unblocked (Velichko, 1987; Velichko et al., 1997). Bolshiyanov (2006) challenged this opinion and introduced the "passive glaciation" concept. In this context, it is assumed that the sea level fluctuations might have created extensive abrasion platforms. Another viewpoint suggests that the forms of relief which previously were considered as glacial and fluvioglacial (moraines and eskers), did not originate from cover glaciations, but resulted from erosion, abrasion, and thermokarst outcrops associated with permafrost-erosion and tectonic processes of the late Pleistocene. It was suggested that isolated parts of Smarovskoye glaciation (300,000 to 230,000 years ago) existed in some areas of the Tyumen region combined with relics of ancient marine terraces (Lazukov, 1972). Later, there was a heated discussion in the Russian geology community regarding the nature of possible glaciations and sedimentation history of Western Siberia. It was suggested that glaciations extended up to Siberian Uvaly that continued as the ancient periglacial Mansyiskoye lake (Grosvald, 1999). Bolshiyanov (2006) suggested that the glaciations were passive, without forming a discontinuous cover or preferential flow blocking in the area topography. At the same time, the abrasion relief with extended ledges was formed in the late Pleistocene period. Finally, the Q-42-43 national geological map indicates that there is a combination of both terrestrial glacial and marine glacial sediments and numerous lake terraces in Western Siberia (Babushkin, 1996). Nowadays, the glacial sediments are excluded from the current version of the national geological map (Faibusovich and Abakumova, 2015) which contradicts the results obtained by Fredin et al. (2012) and Astakhov et al. (2016). Currently, there is no uniform concept of the landforms genesis in Western Siberia. The basing of the Nadym River is considered as most important for the Quaternary interpretation of the local Pleistocene history. The topography and sediments of the Nadym River provide the most information for the study of glacial landforms. Many field investigations and remote sensing operations were completed by multiple generations of researchers, providing a valuable baseline for future studies. The results of studying the Nadym River and adjacent areas, combined with other data, served as a basis for a classification of the Quaternary deposits in West Siberia (Maslennikov, 1998; Sedov et al, 2016; Sheinkman et al, 2016; Rusakov et al, 2018). Nevertheless, the current geological map (Faibusovich and Abakumova, 2015) still has unsolved issues that are highlighted as new geological and geomorphological data are obtained.

The study objective is to summarize the results of detailed lithological, chronostragraphic, petrographic and geomorphological studies conducted in the

95  Nadym River basin, and to identify the origins of the key factors of sedimentation
96  accumulation and topography.
97
98      ***Materials and Methods***
99      Fieldwork was conducted in 2016-2018 in the Nadym River Basin, including
100 the valleys of its main tributaries: Kheygiyaha, Yarudey, Tanlova, Left and Right
101 Khetta. The region is characterized by a moderate human-induced burden. There are
102 main gas pipelines (Urengoy-Pomara-Uzhhorod, Nadym-Punga-Lower Tura, etc.),
103 high-voltage power transmission lines (200, 500 kV), an pipeline from Yarudeyskoe
104 oilfield and the Nadym-Priozernyy road. The survey covered the natural exposures
105 along riverbanks, walls of dry quarries located at the watersheds and river terraces
106 as the most informative terrain features. This paper is based on the results of detailed
107 studies of the five most prominent stratigraphy sections of the upper part of
108 Quaternary sediments (Figure 1). For clarity, the section coordinates, their locations,
109 survey dates and the total thickness of the studied deposits are specified (Table 1).
110
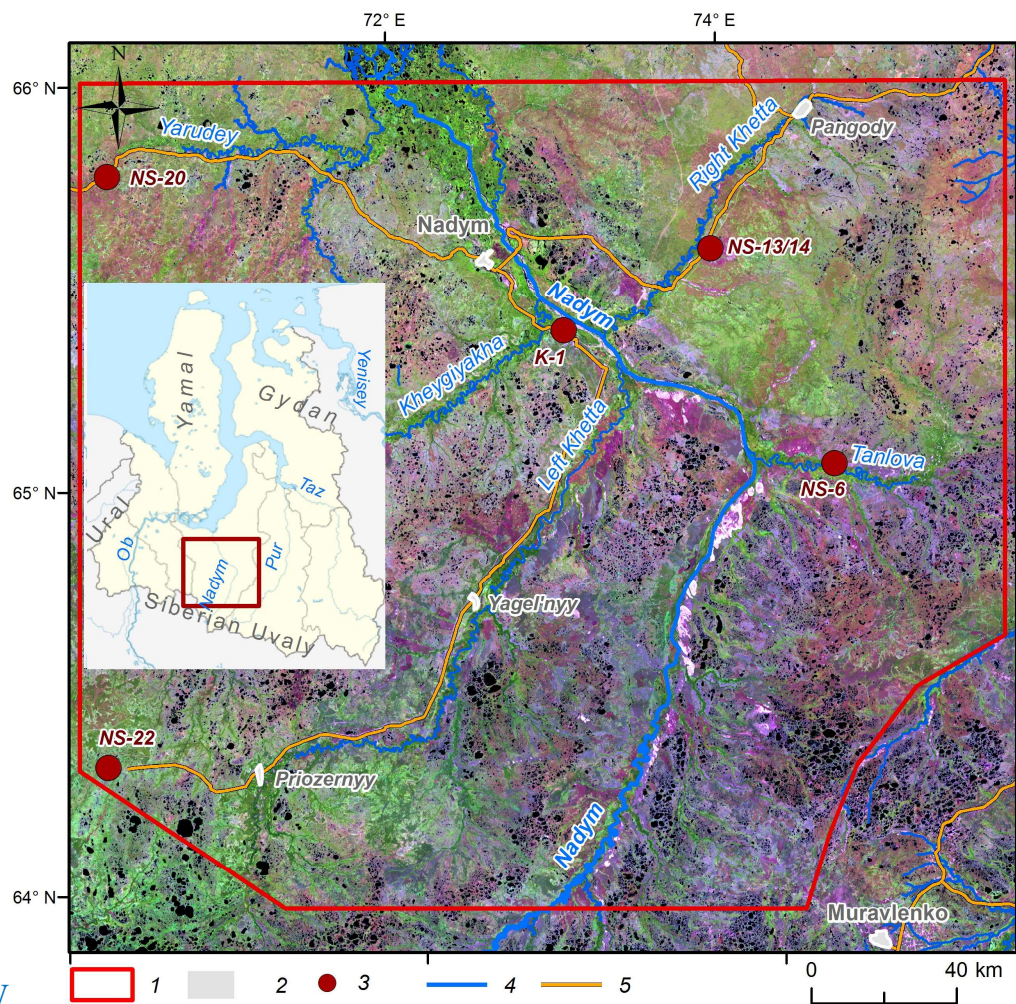
111  NEW
112      Fig. 1. Overview map: 1: study area; 2: settlements; 3: studied and sampled locations; 4:
113                    waterways; 5: roads. Background image: Landsat 8, 2000.
114
115  Table 1
116  Site Properties

| N | Coordinates N, E | Top of sectrion elevation, m a.s.l. | Geogenic location | Sampling point location | Survey date | Thickness, m |
|---|---|---|---|---|---|---|
| K-1 | 65.351044 72.974041 | 24 | Second above flood plain terrace | Wall of quarry | 21.08.2016 | 4.2 |
| NS-6 | 64.974808 74.499714 | 44 | Second above flood plain terrace | River break | 18.08.2017 | 9.5 |
| NS -13/14 | 65.52992 73.875985 | 44,5 | Kamiform hill | Top and slope of hill | 22.08.2017 | 5.1 |
| NS-20 | 65.778072 70.29182 | 57 | Esker sediments | Wall of quarry | 11.08.2018 | 16 |
| NS-22 | 64.31688 70.232456 | 130 | Watershed | Wall of quarry | 13.08.2018 | 1.5 |

117

118     Samples for bulk chemical composition, grain size distribution, sand quartz
119 grain morphoscopy and morphometry, as well as luminescent analysis of sandy
120 textured particles of feldspars were taken from each specified layer of the studied
121 sections in order to clarify the conditions of the sediment formation.
122     The bulk content of oxides was determined by the X-ray fluorescence method
123 at the Analytical Center for Multi-Elemental and Isotope Research, Siberian Branch
124 (SB), Russian Academy of Sciences (RAS), Novosibirsk, Russia, and at the
125 laboratory of the Institute for Physical, Chemical and Biological Problems of Soil
126 Science (Pushchino, Russia). The grain size distribution was determined by
127 conventional fractions separation (sieve analysis) of samples with the Fritsch
128 Analysette 3 vibratory sieve shaker. The fractions were weighed with laboratory
129 scales, 0.1 g accuracy. 17 samples from the sections NS-6 and NS-13/14 were
130 analyzed at the Laboratory of Ground Mechanics, Institute of Cryosphere of the
131 Earth, Tyumen Research Center RAS with the Mastersizer 3000E laser diffraction
132 particle size analyzer (Malvern Panalytical, Britain). Since different laboratories
133 measured the granulometric composition, the figures for the lightest fractions are
134 slightly different.
135     The Altami CM0870-T binocular microscope was used to study the quartz
136 grains (50 grains per sample) taken from the coarse sand fraction. The grain surface
137 morphology was studied with the JEOL JSM-6510LV scanning electron microscope
138 (SEM) using the secondary electron image (SEI) at the Analytical Center for Multi-
139 Elemental and Isotope Research, SB, RAS. According to the technique applied
140 (Velichko and Timireva, 1995), the grain scale was determined using Rukhin (1969,
141 Figure 2) and Khabakov (1946), where 0 is an angular, and IV is a perfectly rounded
142 grain. The coefficients scale of roundness and the grades of dullness (Velichko and
143 Timireva, 1995) were estimated for each sample. The dullness of the grains was
144 determined visually as glossy (shiny), quarter-matte, half-matte, and matte. The
145 grain surface microrelief structure study was based on numerous published
146 diagnostic features found in grains with various genesis and sediment accumulation
147 conditions (e.g. Velichko and Timireva, 1995; Krinsley, Doornkamp, 2011; Vos et
148 al., 2014; Woronko, 2016; Kalinska-Nartisa et al., 2017). The previous studies in

149 Western Siberia that examined sand quartz grain micromorphology covered peat
150 histic sand deposits in the area of Siberian Uvaly, valleys of the rivers Taz and Pur
151 (Velichko et al., 2011) and aeolian sediments of the southern part of Western Siberia
152 (e.g. Sizikova and Zykina, 2015).
153
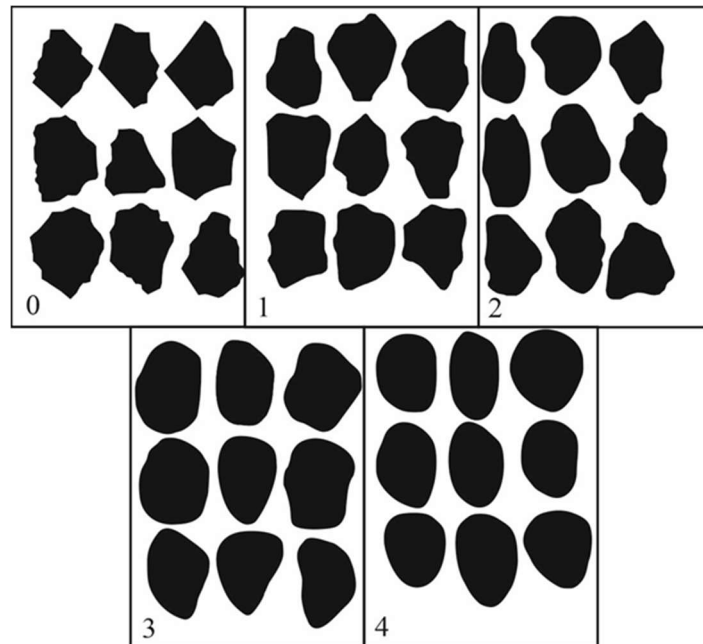
154
155 Fig. 2. Pattern (Rukhin, 1969)
156 0, 1, 2, 3, 4 are the classes of roundness (Khabakov, 1946)
157

158 The potassium feldspar-based infrared optically-stimulated luminescence (IR-
159 OSL) dating method was applied to produce an absolute chronology of the deposits
160 from the five sections studied in the present work. The upper limit of the method is
161 normally 300–500 ka, depending on burial conditions and the physical properties of
162 the mineral. The reliability of the dating technique used in the present study is
163 demonstrated by comparative results obtained using several numerical dating
164 methods (mollusc shell-based electron spin resonance (ESR), quartz-based optically
165 stimulated afterglow (OSA), U-Th and $^{14}$C) applied to the same sedimentary samples
166 (Molodkov, 2012). An overview of the IR-OSL dating procedure is presented by
167 Molodkov and Bitinas (2006). All IR-OSL ages reported in this paper were obtained
168 in the Research Laboratory for Quaternary Geochronology, Institute of Geology,
169 Tallinn University of Technology.
170 In addition to the analysis at the sampling area, samples were taken for
171 petrographic examination. The samples were cut perpendicular to the bedding
172 direction (if any) and made into transparent sections. The Carl Zeiss AxioScope A1
173 optical microscope at the Geology and Mineralogy Institute, SB RAS (Novosibirsk)
174 was used.
175 For the first time for the studied area, digital terrain models (DTM) with
176 spatial resolution of 12 and 26 m/px based on TerraSAR -X and TanDEM -X radar
177 data were used to characterize the geomorphological structure. The mapping is based
178 on the remote features available in the literature (Atkinson et al., 2014; Astakhov et
179 al., 2016, etc.) and the comparison of the field and remote sensing data (Table 2). In

180   addition, public multi-spectrum space images from Sentinel-2 (10 m/px.) were used
181   to clarify the location of such natural features as rivers, lakes, swamps, and forests
182   (https://scihub.copernicus.eu/).
183

184   Table 2
185   Remotedly sensed features of glacial and fluvioglacial relief

| Relief features | Remotedly sensed features |
|---|---|
| Kame-like hummocks | Irregularly scattered hills and ridges with their relative elevation not exceeding 10-20 m. The hills have plateau-like summit, the slopes are gently convex, the slopness varies. The hills and ridges are easily identified on the DTM agaist the flattened background; often they are separated by no-outflow basins and hollows. The hills are at the highest parts of the watersheds and often from groups or even curved chains oriented NE to SW, or E to W. Sparse vegetation areas are associated with the highest parts of the hills. |
| End moraines | Mostly associated with the watersheds. They are narrow, tortuous upheavals (relative elevation is up to 5-7 m, sometimes to 10 m). The survival rate varies. They van be in the form of high linear upheavals with steep clopes to low kettelbacks 10-12 km long. With high resolution DTMs (2-10 m), the small local boaundary moraine formations are easily identified; for mid-resolution DTMs (25-30 m) the large features with a low survival rate are identified. The key properties are the length and the position: the flat moraine pattern usually forms an interconnected structure that reflects the ice sheet extents and the stages of its degradation. |
| Parallel ridges | As opposed to the terminal moraine ridges, the linear ridges are smaller and shorter while their direction is more pronounced (almost no bends.) When ridges are poorly expressed, an additional indicator is a linear structure of the multispectral image caused by the similar orientation of the river valleys, chains of small lakes, forest and bog boundaries.. |
| Valley trains | Twisted similarly to smooth river meanders. Nowadays they are swamped and turned into lakes. Merging and splitting, they form a typical pattern of the hydrographic network. The valleys are often associated with expected drainwater sources mostly located in glacial accumulative formations on the watersheds. The valleys often terminate with chains of lakes perfectly visible in satellite images. |

186

187   **_Results_**

188

189   *Characteristics of the Sections*
190         The summary results of the Quaternary sediment section study are shown in
191   Figures 3-7 and Annexes 1, 2. From the data obtained, the following characteristic
192   conditions of sediment accumulation can be distinguished:
193
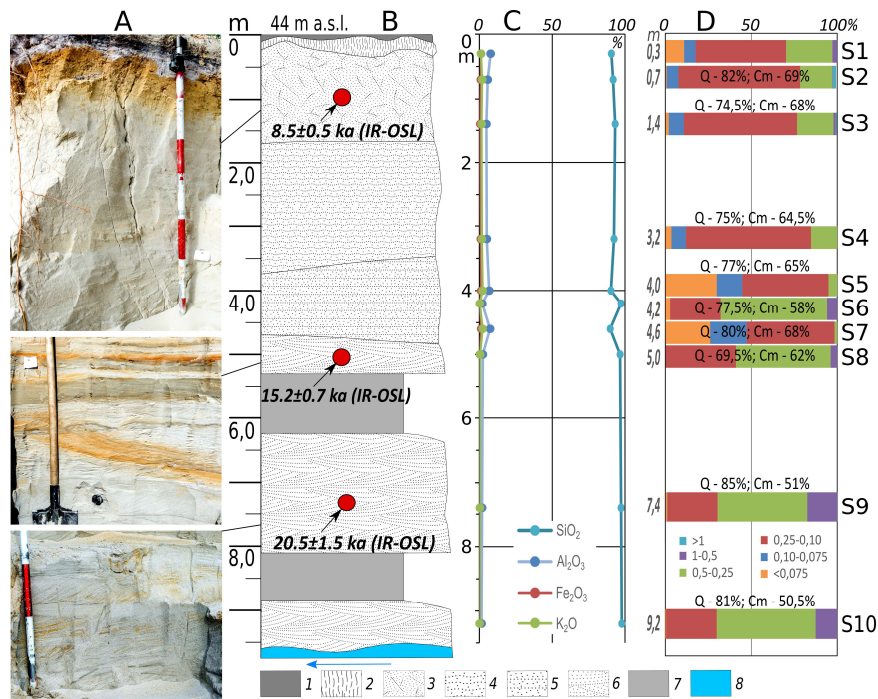
194
195 *Fig. 3. Summary results of research for section NS-6. A: photographs (by Sizov in 2017); B:*
196 *geological structure and the dating results (refer to Table 3); C: bulk chemical data; D: grain size*
197 *distribution (fractions, mm). Symbols: 1: podzol horizon of modern soil; 2: illivial-iron (spodic)*
198 *horizon of modern soil; 3: sands without stratification; 4: undulating sand with secondary ironing;*
199 *5: horizontally layered sand with stratification of loam; 6: medium-and coarse-grained oblique*
200 *sand; 7: colluvium; 8: river level; Q: coefficient of roundness of the sand quartz grains; Cm:*
201 *degree of dullness; S: sample number.*

202

203
204 *Fig. 4. Summary results of research for section K-1: A: photographs (by Sizov in 2016);*
205 *B: geological structure and the dating results (refer to Table 3); C: bulk chemical data; D: grain*
206 *size distribution (fractions, mm). Symbols: 1: podzol horizon of modern soil; 2: illivial-iron*
207 *(spodic) horizon of modern soil; 3: sands without stratification; 4: undulating sand with*
208 *secondary ironing; 5: horizontally layered sand with stratification of loam; 6: medium-and*
209 *coarse-grained oblique sand; 7: colluvium; 8: river level; Q: coefficient of roundness of the sand*
210 *quartz grains; Cm: degree of dullness; S: sample number.*

211
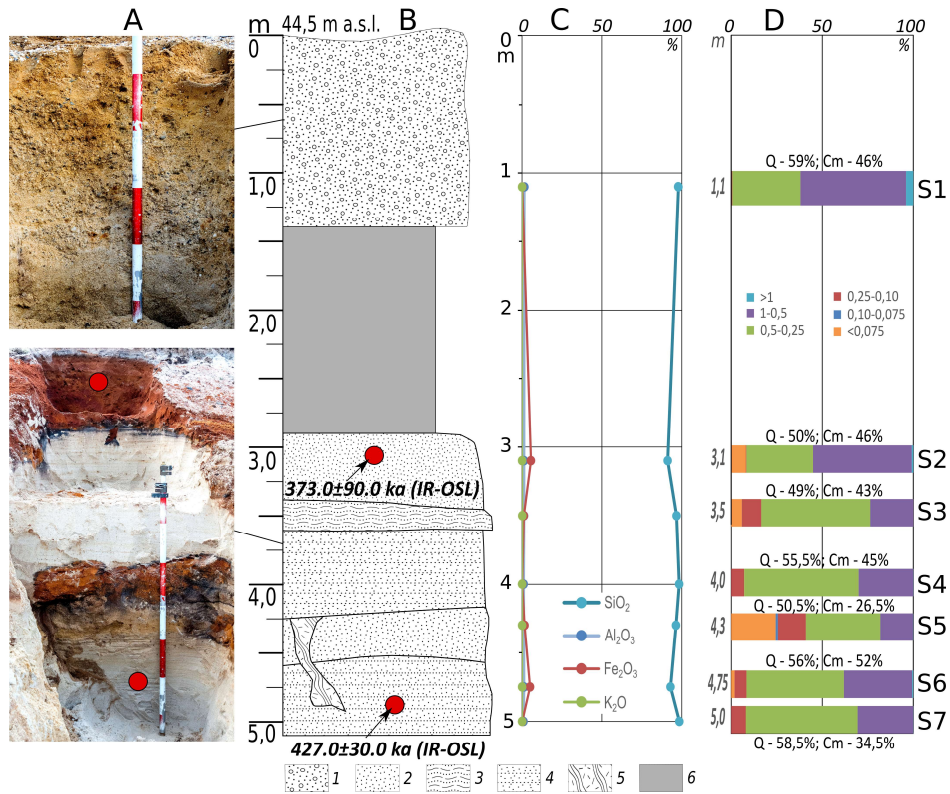
Fig. 5. Summary results of research for section NS-13/14: A: photographs (by Sizov in 2017); B: geological structure and the dating results (refer to Table 3); C: bulk chemical data; D: grain size distribution (fractions, mm). Symbols: 1: coarse sand with pebbles; 2: unstratified red sand; 3: undulating black sand; 4: horizontally layered sand; 5: wedge filled by deposits of the overlying layer; 6: colluvium; Q: coefficient of roundness of the sand quartz grain; Cm: degree of dullness; S: sample number.
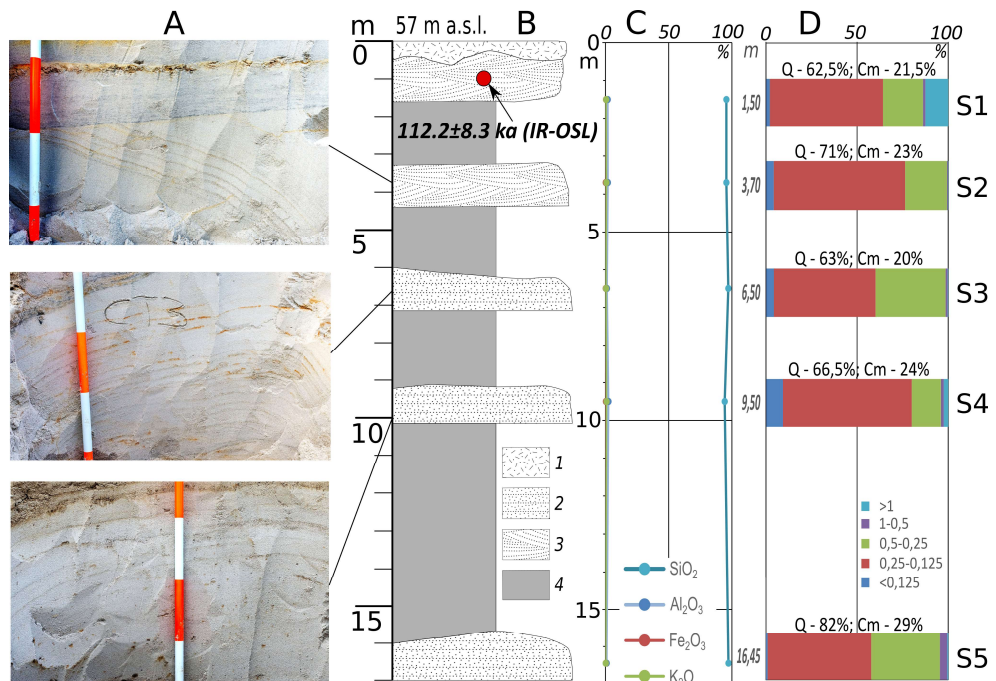
Fig. 6. Summary results of research for section NS-20: A: photographs (by Sizov in 2018); B: geological structure and the dating results (refer to Table 3); C: bulk chemical data; D: grain size distribution (fractions, mm). Symbols: 1: overburden; 2: horizontally layered sand; 3: medium-and coarse-grained oblique sand; 4: colluvium; Q: coefficient of roundness of the sand quartz grains; Cm: degree of dullness; S: sample number.
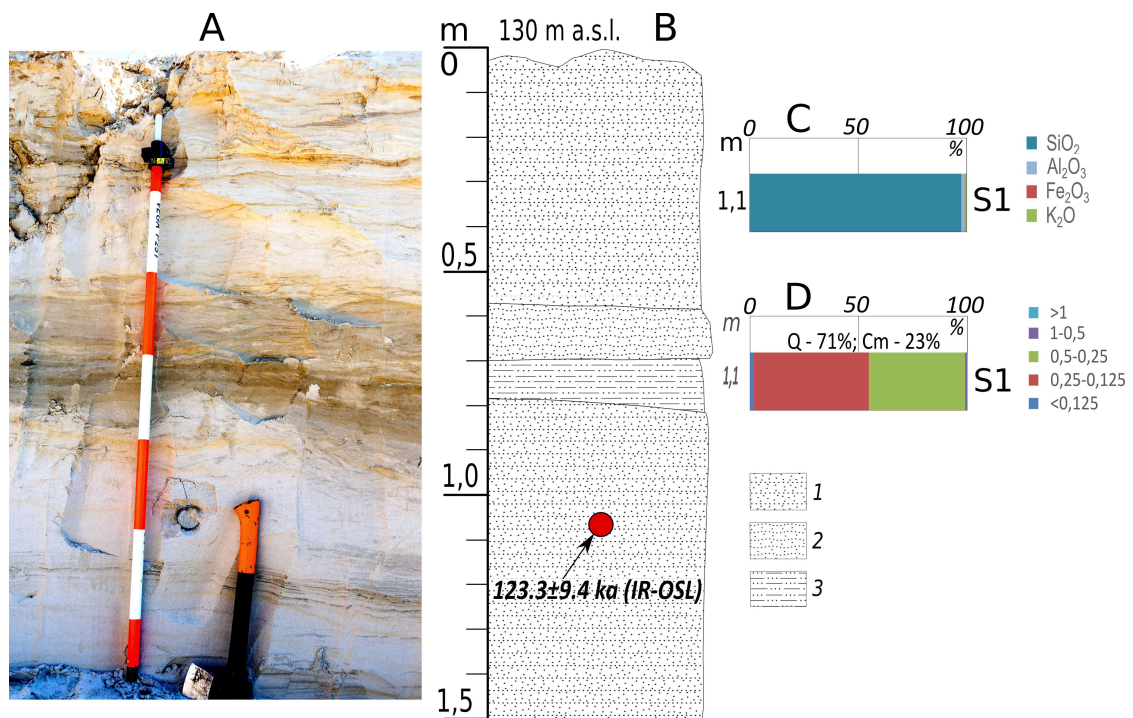
Fig. 7. Summary results of research for section NS-22: A: photographs *(by Sizov in 2018)*; B: geological structure *and the dating results (refer to Table 3)*; C: bulk chemical data; D: grain size distribution (fractions, mm). Symbols: 1: horizontally layered grey sand; 2: oblique layered sand; 3: horizontally layered sandy loam; Q: coefficient of roundness of the sand quartz grain; Cm: degree of dullness; S: sample number.

1. Alluvial deposits predominate at the lower geomorphological level (up to 40-45 m.). Sections K-1 and NS-6 show the similar structure of the second above-ground terrace of the Nadym and Tanlov rivers: in the upper part, thick podzolized soil is formed over the aeolian deposits; in the middle part, floodplain type deposits dominate; and in the lower part they are replaced by well-leached gray layered sand. Down the profile, the $SiO_2$ content increases, while the content of other chemical elements is low. The middle part of the section is dominated by fine and medium-grained sand, the portion of large fractions increases in the lower part where single pebbles with diameters up to 3-4 cm are found. There are no permafrost-affected sediments.

2. At the middle topographical level, the sections show the structure of a NS-13/14 kamiform hill and a linear-oriented relief (NS-20). The top of the hill is covered with a solid layer of pebbles; at 1.2 m depth, it is followed by coarse sand. Sandy deposits forming two distinct cycles are exposed in the middle part of the hill. The unbroken red-colored sand is followed by black sand with slightly horizontal orientation, which in turn is followed by light-grayish horizontally layered sand. In the lower profile, the cycle is repeated; the difference is that the layer of intensively reddish sand is not as thick. In the left lower part of the section, there is a frost wedge microdepression, filled with the overlying layer sediments. In general, the section is dominated by medium- and coarse-grained sands of monomineral composition (the shares of Fe, Al and other chemical elements are insignificant).

In section NS-20, the slope of the extended elevation is exposed. It is composed of a monotonic body of grey monomineral parallel and oblique-oriented

quartz sand. The sands throughout the section have an identical grey color and fine-grained composition. The presence of thin iron-containing layers does not affect the chemical composition of sediments: $SiO_2$ prevails in all layers. Local hills up to 5-8 m high covered with large pebbles and boulders on the surface were found on the top of the ridge along the survey path. In an exploration ditch on the top of the microhill (1.5 m deep), large-grained, non-laminated sandy sediment with the abundance of angular pebbles, gravel, and single large (diameter up to 30-40 cm) boulders were exposed. Their structure is similar to the deposits of the upper part of section NS-13/14. In none of sections, permafrost sediments or traces of frost cracking occur.

3. The NS-22 is at the upper watershed in a small quarry. The qyarry exposes sandy and sandy-loam bedded deposits of the large hill on the upper topographical level. Sands in the sample are grey-colored, fine and medium-grained. The $SiO_2$ content is 96.49%. A huge number of large, weakly rounded boulders, diameter up to 1.5 m in size, was found in the quarry and on the sandbank of the nearest lake (100-200 m from the quarry).

It should be noted that grey fine, medium- and coarse-grained sands of monomineral quartz composition are present in all sections (except for NS-13/14). In river terraces, such sands have oblique lamination, while on the watershed they are oriented horizontally. The sands have no permafrost features, cracking traces and, in general, poor chemical composition. A landscape vegetation feature of such sediments is pine sparse forests, which are able to grow on poor sandy soils with a well-drained hydrologic behavior. Sandy soils lack organic materials and debris of fossil clams, and do not show any salt content. Despite the presence of large debris on the scree slopes; boulders do not occur directly in the sands. Based on morphological, particle size and chemical features infer we infer that this type of sand sediment could be formed in subaquatic conditions in more severe environments as compared to modern climatic conditions. This is also confrimed by correlation coefficient value – quartz content is negative correlated with key oxides in bulk compostion of the fine earth (Annex 2).

### 3.2. Sediments Dating Results

IR-OSL ages for the sediment samples from the sites studied and the related analytical data are listed in Table 3.

Table 3
Absolute dating by the IR-OSL method

| Section | Sampling depth (m) | Sample code | Age (ka) | U (ppm) | Th (ppm) | K (%) |
|---|---|---|---|---|---|---|
| K | 3.15 | RLQG 2443-057 | 24.3 ± 1.7 | 0.11 | 0.45 | 0.01 |
| NS-6 | 1.0 | RLQG 2563-019 | 8.5 ± 0.5 | 0.79 | 0.73 | 0.94 |
| NS-6 | 5.0 | RLQG 2564-118 | 15.2 ± 0.7 | 0.01 | 0.00 | 0.14 |
| NS-6 | 7.3 | RLQG 2565-118 | 20.5 ±1.5 | 0.01 | 0.00 | 0.14 |
| NS-13/14 | 3.1 | RLQG 2567-019 | 373.0 ± 90.0 | 0.00 | 0.00 | 0.00 |
| NS-13/14 | 4.9 | RLQG 2568-019 | 427.0 ± 30.0 | 0.35 | 0.74 | 0.00 |
| NS-20 | 1.1 | RLQG 2577-059 | 112.2 ± 8.3 | 0.96 | 4.19 | 0.34 |

| NS-22 | 1.0 | RLQG 2578-059 | 123.3 ± 9.4 | 1.29 | 2.00 | 1.31 |

From section K-1, a single date of 24.3±1.7 (RLQG 2443-057) was obtained at the depth of 3.2 m. According to this age, sediment deposition took place at the very end of the third (Lipovka-Novoselovo) warm phase, which was recorded in the north of Western Siberia during MIS 3 (Marine Isotope Stage 3) by both the [14]C (Kind, 1974) and clam shell-based ESR (Molodkov, 2020) methods.

The normal sequence of the youngest ages of 20.5 ka (RLQG 2565-118), 15.2 ka (RLQG 2564-118), and 8.5 ka (RLQG 2563-019) was obtained for section NS-6 at the depths of 7.3 m, 5.0 m, and 1.0 m, respectively. Specific analytical features suggest the supply of the sedimentary rock from the same source area. The genesis of the deposits is also identical. It implies similar conditions for the rock transfer despite the likely difference in climatic conditions.

Somewhat unexpected were the dating results for two consecutive layers in section NS-13/14: 427.0 ka (RLQG 2568-019) and 373.0 ka (RLQG 2567-019). Finding very old Pleistocene deposits (MIS 11) is exceedingly rare. Judging from the analytics, the sedimentary rock in these layers came from different source areas and has fluvial, most likely river genesis. Under the given conditions of burial and physical properties of the mineral, the upper dating limit may be at least three times higher (i.e., up to about a million years).

The last two datings at 123.3 ka (RLQG 2578-059) and 112.2 ka (RLQG 2577-059) were obtained from two sections: NS-22 and NS-20, respectively. Their common feature is that both of them fall into MIS 5, as well as the fact that the corresponding sedimentary rock also came from various source areas. The studied sediments on the base of a group of key features are supposed to have fluvial (river and lake) origin.

*3.3. Sand Quartz Grain Morphoscopy and Morphometry.*

Refer to Annexes 4-13 for the key results: coefficient of roundnesss, degrees of dullness, and examples of the quartz grain appearance. The following is a brief description of the main features.

NS-6. Aeolian genetic group. The upper part of the section (samples S2 and S3) is characterized by a high coefficient of roundnesss (Q; 74.5 - 82%) and degree of matting (Cm; 68 - 69%). IV rounding class matte grains prevail; the complete grain distribution vs. rounding and surface dullness are shown in Annex 4. The most common element of grains microrelief in the S1 sample is a micro-pitted surface (Annex 9 a, b), which is a feature of aeolian transportation (Velichko and Timireva, 1995). Chemical etching is sometimes found in depressions. High coefficients of roundness (Q) and degrees of dullness (Cm) along with the predominance of micro-pitted grain texture suggest the dominance of aeolian processes during the sedimentation. Several grains show signs of subaquatic treatment and origin in the form of crescentic depressions and V-shapes percussions (Annexes 9 a, b), which preceded the aeolian stage. It seems to be associated with the accumulation of rock from the river valleys.

337     For quartz grains from the floodplain deposits (samples S4-S8), the rounding
338     coefficient (Q) is within the range of 65-80%; the degree of dullness (Cm) is 58-
339     68% (Figure 3). On average, IV rounding class grains (Refer to Annex 4) with a
340     half-matte surface prevail in the samples. The number of completely glossy grains
341     increases (up to 22%). The entire grain surfaces have signs of subaquatic processing:
342     V-shaped percussions (Annex 9 d), often forming a fine-pitted surface (Annex 9 c,
343     d), and separate crescent gouges. Many grains show traces of aeolian treatment,
344     expressed as a micro-pitted texture (Annex 9 c), which corresponds well to a
345     sufficiently large share of matte grains in the sample. It can be assumed that deposits
346     of this layer are formed by fluvial river and aeolian processes in the coastal
347     environment.
348     For samples from the lower part of the section (samples S9, S10) Q = 81-85%
349     and Cm is 50.5-51%. Most grains belong to the IV rounding class. The number of
350     glossy grains (up to 32%) is significantly higher than in overlying sediments (Annex
351     4). The primary grain treatment traces on the surface of all grains, regardless of the
352     roundness and dullness, are fine-pitted surfaces (Annex 9 e, f) and individual well-
353     developed V-shaped microdepressions (Annex 9 f), which is a sign of active river
354     fluvial transportation. There are grains of the II and III classes of roundness; they
355     differ from most grains by the presence of flat faces (Annex 9 g, h). The shapes of
356     these grains resulted from the previous stages of grain treatment. There are also signs
357     of aqua tic treatment on its surfaces (Annex 9 g, h).
358     The K-1 grain distribution across the section matches well the morphometric
359     and morphological properties of the NS-6 section (see Annex 5 for the grain
360     distribution by roundness and dullness). Samples S6-S7 lying in the base of the
361     section provides important information. These samples differ in grain morphology
362     from overlying sediments. They are characterized by the lowest cross-sectional
363     values of the coefficient of roundness (63-65%) and the degree of matting (33-35%),
364     the presence of glossy grains in all classes of roundness (Annex 10), constrained or
365     ground flat faces at grains, and the development of sickle-like texture and fine pits
366     on the grain surface. With these features, it can be concluded that this layer was
367     formed by fluvial processes, but it should be emphasized that there is a rock in its
368     composition that may have been exposed to glacial processes in the past.
369     NS-13/14. For S1 deposits Q= 59% and Cm = 46%. Angular grains, class I
370     (32%) and medium-rounded grains, class II (24%) predominate. Most grains have
371     half-matte (34%) and quarter-matte (32%) surface (Annex 6). The grains can be
372     categorized into two groups. The first group is represented by well-rounded mature
373     grains with a ubiquitous fine-pitted surface (Annex 11 a), which is a sign of
374     treatment by aqueous streams. In the second group, there are grains of irregular
375     shape (Annex 11 b), often with multiple or conchoidal fractures. The faces have
376     traces of treatment in subaquatic environment. Grains of the second group show
377     separate V-shaped and rarely crescentic-shaped percussions; their number and
378     location indicate a lower exposure to water flow. The presence of these two different
379     groups of grains suggests the ingress of rock from different sources of the rock. One
380     one them could be the subangular fluvioglacial deposits.

For underlying deposits (S2-S7) Q=49 – 58.5% and Cm=26.5-52%. There, poorly-rounded and middle-rounded grains of classes I and II with a glossy or quarter-matte surface prevail (Annex 6). The grain surface is dominated by traces of low-activity subaquatic treatment: V-shaped and crescentic microdepressions (Annex 11 c-h). Irregular grains with smooth surfaces are most common, often with fractures (Annex 11 e, f, h), which probably indicates its arrival from a source with poorly rounded materials. There are grains with conchoidal fractures formed by desquamation processes due to grain freezing (Velichko and Timireva, 1995) or under a big pressure applied to the grain (Immonen et al., 2014; Vos et al., 2014.) There are also V-shaped percussions along its surface, suggesting that the deformation occurred before the last fluvial treatment. Many grains were highly exposed to chemical processes expressed as etching through the depressions on the grain and the Fe-Mn skins. The development of V-shaped forms only along the protruding parts of the grain, a well-developed crescentic-shaped texture and non-ubiquitous fine-pits, the average values of the coefficient of roundness and low degrees of maturation suggest that the final processing of grains occurred in a relatively calm aquatic environment. For S2 and S3 samples, in addition to traces of subaquatic treatment, there are grains with small micro-pits (Annex 11 c, d), a sign of aeolian treatment of grains.

NS-20. For samples S1-S5, the coefficient of roundness (Q) is in the range of 62.5-82% and the degree of dullness (Cm) is 20-29%. Glossy grains of II and III classes of roundness prevail (Annex 7). In the most most sediments (S1), there are signs of aeolian treatment of grains expressed as micro-pits (Annex 12 a, b). However, they have a rather low value of Cm, which is not typical of aeolian deposits. This suggests that the local aeolian redeposition of underlying sediments occurred. The underlying layers (S2-S5) have sediment features; their formation is probably associated with fluvioglacial processes: the surface of most grains is highly uneven, cavernous, and strongly mechanically deformed. These properties can be found in glacial conditions (at the stages of previous processing). This is also suggested by the presence of deep-pits, grooves and parallel scratches of various configurations (Annex 12 c, d, h). The last agent in their treatment was a subaquatic process, as indicated by frequently occurring V-shaped and crescentic depressions (Annex 12 e, f, g).

NS-22. The coefficient of roundness (Q) is 79% and the degree of dullness (Cm) is 31%. Most of the grains belong to class III of roundness, a slightly smaller number of grains are of class IV; glossy grains prevail (Annex 8). The morphology of the grain surface is quite uniform and is mainly represented by grains with fine pits covering the grain surface almost completely (Annex 13 a-f) or developed only on microelevation parts of the grain (Annex 13 e, f). This surface is a characteristic feature of the long-term grain processing in a sufficiently active subaquatic environment.

*3.4. Petrography*

The petrographic analysis of 15 samples taken in a quarry nearby the section AS-3 (Figure 8, coordinates: N65.061417°, E72.943848°) enabled to distinguish several groups of materials:

1) The first group (6 samples) is presented by grey, yellowish-grey, and greenish-grey fine-grained and very fine-grained sandstone and siltstone with slab jointing. They are usually moderately or poorly sorted and have primary foliation that is emphasized by the regular orientation of flattened grains, varying grain size, and matrix content. The matrix is hydromicaceous clay, sometimes with ferruginous cement, with a small portion of silica. The fragments are usually sub-rounded or sub-angular. The rock is composed of polymictic sandstones, similar to arkoses sandstones. Quartz and feldspar prevail among the mineral grains, composing ~30 vol% of the fragments, while another third is predominantly composed of siliceous rock fragments. Some samples contain significant amounts of muscovite (up to 5% by volume), chlorite (including pseudomorphs after the dark-colored minerals), and epidote. The presence of muscovite could be an indicator of low weathering of initial sediments.

2) Pebbles and boulders of the second group of quarzitic and quartz sandstone (6 samples) feature angular forms. The textures are usually massive and vary from poorly to well sorted. The cement is predominantly quartz or quartz-hydromicaceous, sometimes with goethite. The grain size varies greatly, but medium-sized varieties prevail. More than 95% of grains are quartz and siliceous lithoclasts, while muscovite, feldspar, epidote, zircon, monazite, and opaque minerals are also present. The quarzitic sandstones show regenerative incrustations around the primary rounded quartz grains. The grain boundaries are most often irregular and frequently saw-shaped, which indicates a notable meta-genetic alternation. Late veins of the fine-grained quartz aggregate are also rather frequent.

3) The third group of samples was the least numerous yet the most informative. In this case, the first sample is a cobble of pinkish quartz trachyte–alkaline intermediate volcanic rock. Large pelletized phenocrysts of potassic feldspar (up to 1 cm) and rare fine quartz grains are distributed in the groundmass composed of pelletized potassic feldspar and quartz (Figure 8 a). Furthermore, quartz-feldspathic myrmekites are rather frequent. There are small quantities of plagioclase, dark-colored minerals that are substituted by aggregates of chlorite, epidote, and opaque mineral.

The second sample is dolerite with typical poikilitic texture (Figure 8 b) formed by large poikilite clinopyroxene crystals (3-4 mm in diameter) with tabular plagioclase (up to 1-1.5 mm). There are large, separate hypidomorphic crystals of basaltic hornblende (up to 2 mm), which are substituted by hydrous ferric oxides, titanite, and chlorite. The main groundmass contains plagioclase and significant amounts of chlorite, which is presumably a product of substitution of the volcanic glass or clinopyroxene microliths.

The third sample is zoisite-amphibolite (zoisite-actinolite) metasomatic rock. Light-green idiomorphic grains of amphibole prevail over hypidomorphic crystals and sheaf-like aggregates of zoisite. Anhedral segregations of titanite and opaque

468  ore minerals are also present. From a general chemical perspective, it can be
469  suggested that the most probable protolith for this rock was a dolerite-like rock.
470
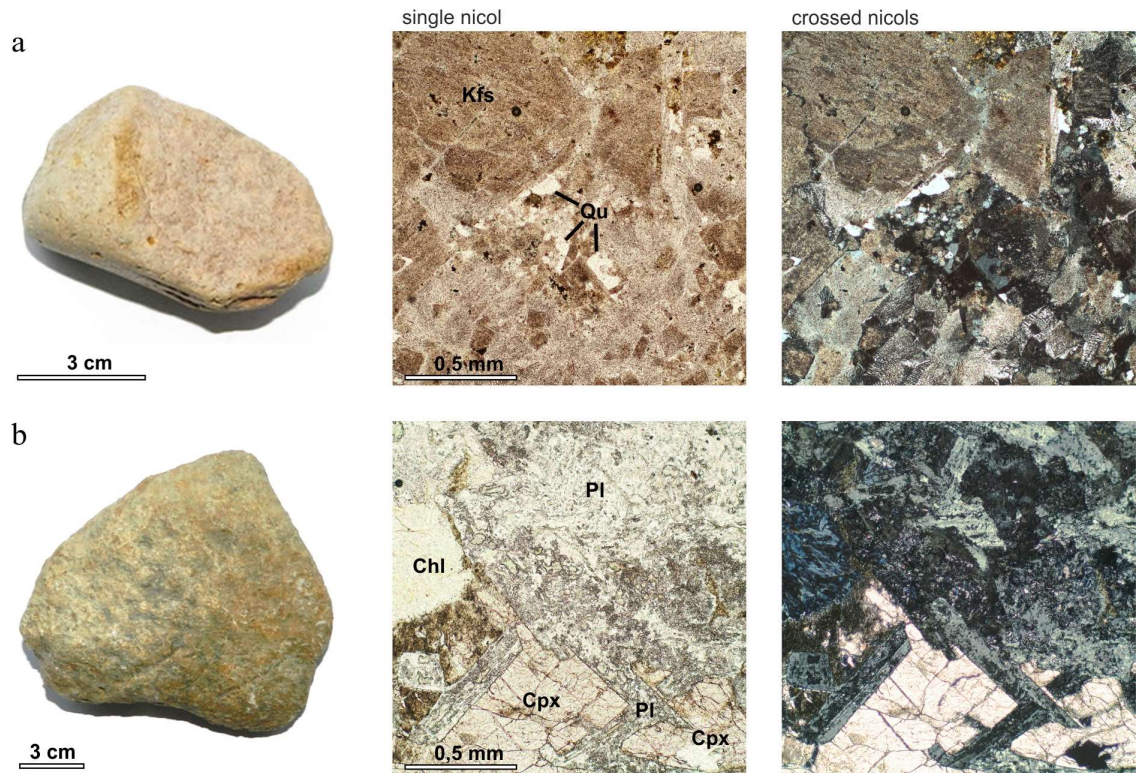
471  NEW
472  Fig. 8. (a) Sample N-10 – pinkish quartz trachyte, large inclusions of potassic feldspar (Kfs) with
473       fine quartz grains (Qu) in the quartz-feldspathic matrix; (b) sample N-14: greenish-brown
474   dolerite, large poikilitic clinopyroxene crystals (Cpx) with thin plagioclase crystals (Pl), in the
475                    groundmass: plagioclase chlorite (Chl).
476

477      *3.5. Geomorphological Analysis*
478       The investigated area is in the zone of sparse northern taiga with extensive
479  peatlands. Therefore, the existing digital surface model (DSM), based on X-band
480  radar data with high penetration capacity, reflects in detail the terrain structure of
481  the territory. DEM mapping of the glacial ice and fluvioglacial relief features was
482  performed using a site with an area of 54,117 km$^2$ as an example. Its boundaries run
483  along the watershed of the Nadym River and its tributaries. The summary mapping
484  results are shown in Table 4 and Figure 9.
485

486  Table 4
487  Remote mapping of the glacial and fluvioglacial relief features in the Nadym River basin (mid
488  and lower courses)

| Relief features | Number of identified objects | Total area/length, km |
|---|---|---|
| Kame-like hummocks | 157 | - |
| End moraines | 122 | 851.3 |
| Parallel ridges | 16 | 157.2 |
| Valley trains | 103 | 1411.3 |

489
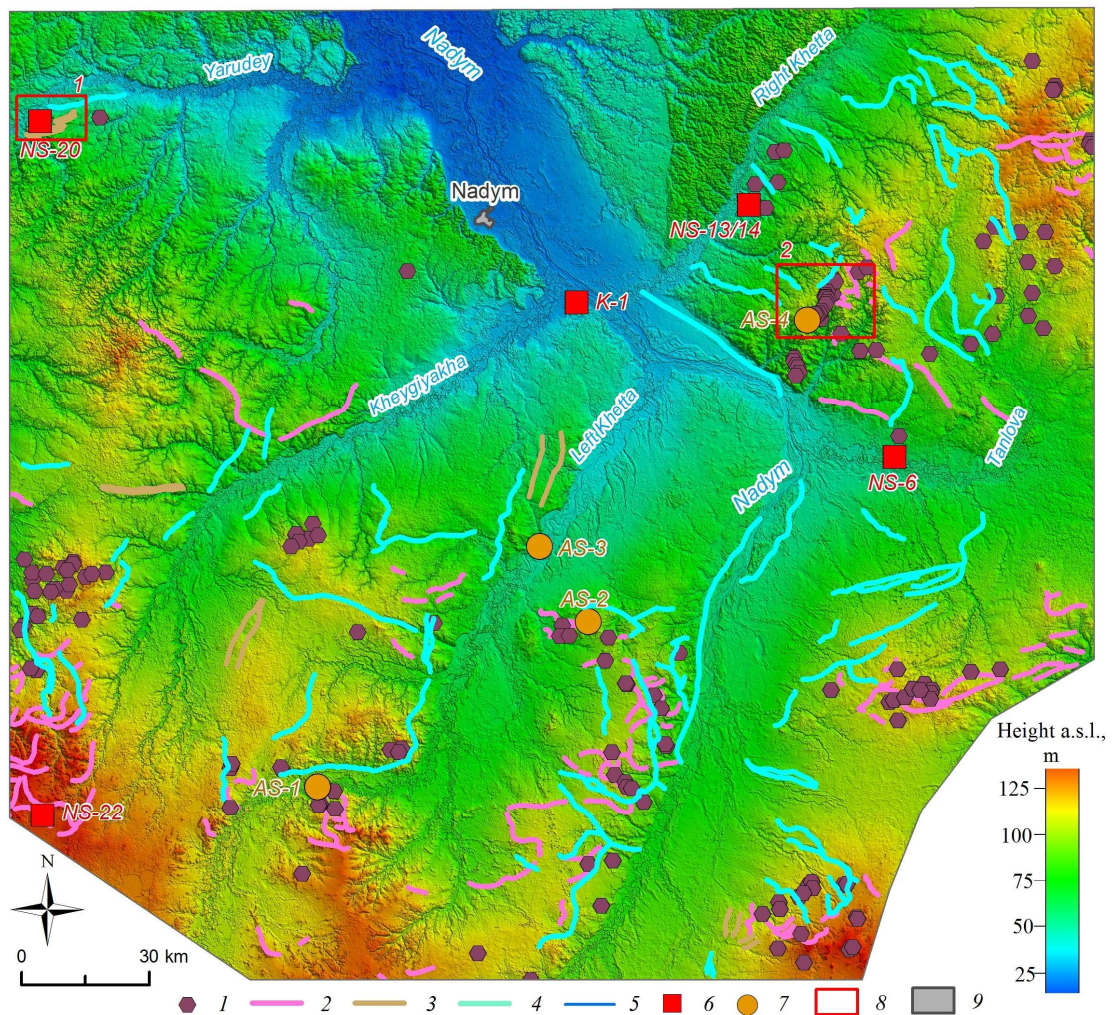
Fig. 9. Results of the glacial and fluvioglacial relief interpretation in the middle course of the Nadym River (the background image is a synthesized digital terrain model based on DEM TanDEM-X, 26 m resolution): *1: kame-like hummocks; 2: moraines; 3: parallel ridges; 4: valley trains; 5: waterways; 6: studied and sampled locations; 7: additional locations based on Khlebnikov, 1954; Yevseyev, 1958; 8: areas of typically glacial landforms; 9: settlements*

Based on the map obtained (Figure 9), it can be noted that the spread of the assumed glacial and fluvioglacial relief features within the investigated area has two distinct patterns:

– all identified features are to the south off the Yarudey and Right Khetta rivers, with individual objects found in the watershed between Yarudey and Kheygiyakha. In the southern and western parts, the diversity and density of the features are the highest (Tanlova and Right Khetta rivers watershed, left bank of the Nadym River in its middle course);

– all identified features are found at the heights from 40 m a.s.l. and higher; the density of objects significantly increases in the watershed areas above 70-75 m a.s.l.

The feature of the high elevation relief distribution is demonstrated by the statistical data about the selected kameform hills. Among the 157 point objects, 145 (92%) are above 75 m a.s.l., with 53 (34%) located within the narrow range of 95-104 m a.s.l. Below 75 m a.s.l., large objects occur individually and are poorly distinguished morphologically.

The network of extended (more than 850 km) end moraines that mark the final glacial massif positions is confidently recognized. They have different stretches (sub-latitudinal, north-western, etc.), which may indicate there was no single direction of the cover ice movement. In most cases, the moraines are confined to the watersheds, while they are often accompanied by other glacial forms (kames, valley trains, etc). The chain of kame hills on the watershed of the Tanlova and Right Khetta Rivers are erosive remnants of the local moraine formations, i.e. morphologically they occupy an intermediate position between the individual moraines. On the watersheds, well-drained, dry areas of sands near kame ridges are often subjected to deflation and active redispersal.

Some of the individual objects are linear ridges (about 157 km total length). The linear ridge relief also has visible signs of erosion (scours, rills, subsidences) and in most cases can be traced as a specific linear landscape texture.

The valleys and rills of the melt glacial waters flow are more than 1,400 km long. The valleys are well expressed in the southern and eastern parts of the study area and are barely visible below 40 m asl. The network of valleys does not really match the modern watercourses; they can be located both in parallel at a small distance from the ancient valleys, or intersect them at right angles. The valleys and hollows of the ancient runoff are often associated with terminal formations. The preservation of valleys is one of the key signs of marine transgression absent in the middle course of the Nadym River since the last glaciation of the region.

For clarity, two sections of typically glacial landforms are highlighted on the map (Figure 9):

1. A site with a predominant linear ridge relief, located on the right bank of the Yarudey River (left tributary of the Nadym River), near the Nadym-Salekhard highway under construction (Figure 10). Four long, curved ridges reaching a height of 55 m a.s.l. are well-preserved (the difference in relative heights is 10-12 m). To the south of the ridges stands a section of hilly, presumably kame, relief. The ridges are complicated by thermokarst and erosion features.

2. The kame hill concentration site on the right bank of the Nadym River, (Figure 11). The kames reach an absolute height of more than 100 m a.s.l. (difference in relative height up to 30 m). The kames are well preserved despite the destruction of individual features by the river erosion.

### *Discussion*

According to current viewpoints, the territory of the north of Western Siberia was exposed to several cover glaciations: Zyryanka (MIS 4), Taz (MIS 6) and Samarovo (MIS 8). Areas at the lower level (up to 40-45 m a.s.l.) could represent serial repeated marine transgressions in Kazantsev (MIS 5) and Karga (MIS 3) ages. The glaciation boundaries are presented in Figure 12. The correlation of the main palaeoenvironmental events in the Western Siberia with those on the East European Plain is presented in Figure 13. Directly within the boundaries of the investigated areas the boundaries of Taz (MIS 6) and possibly Zyryanka glaciation periods are identified (Zemtsov, 1976; Babushkin, 1996).
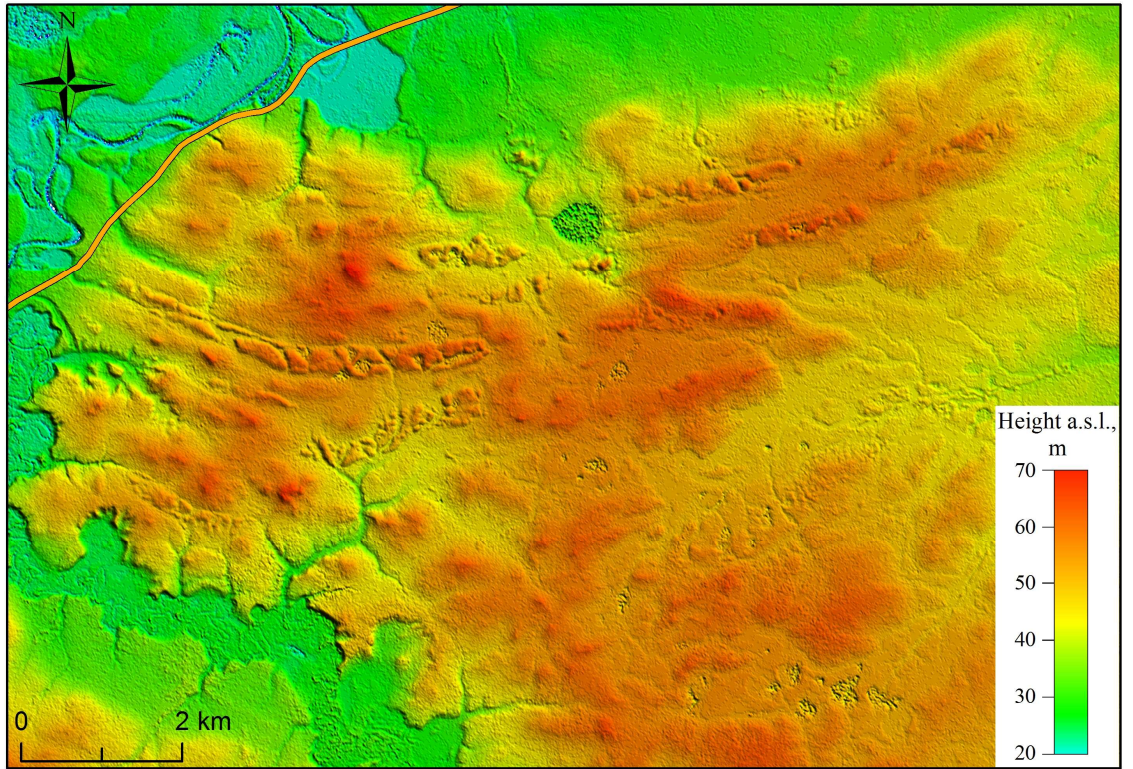
558      ——— Nadym-Salekhard highway
559                     Fig. 10. Parallel ridges, DEM TanDEM-X, 12 m / px.
560
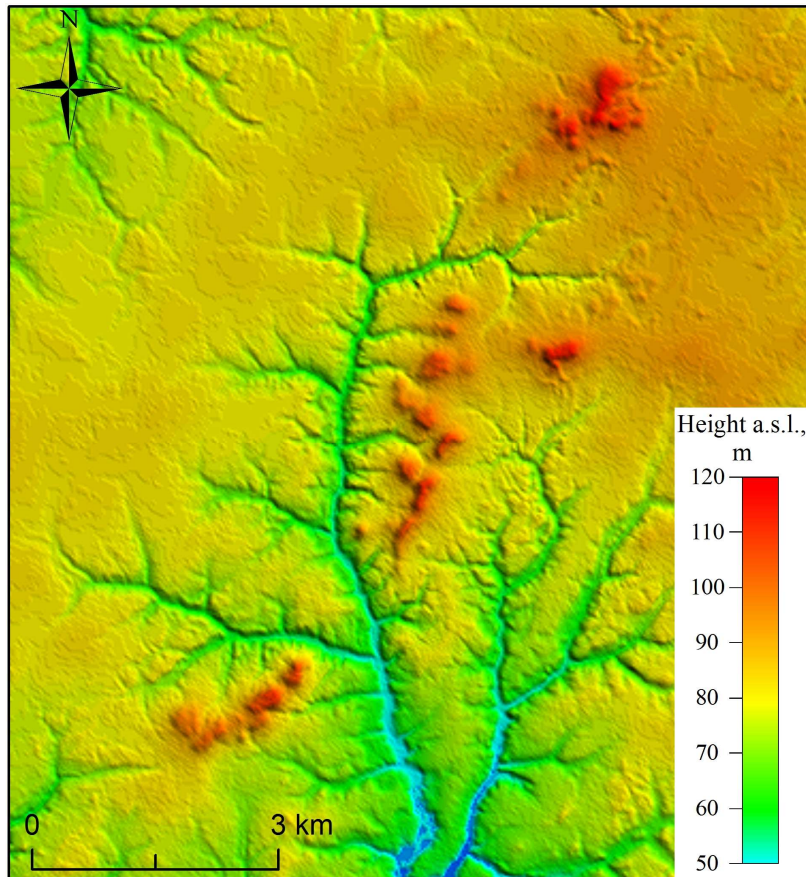
561             
562             Fig. 11. Kame-like features, DEM TanDEM-X, 26 m / px.
563
564

565 NEW
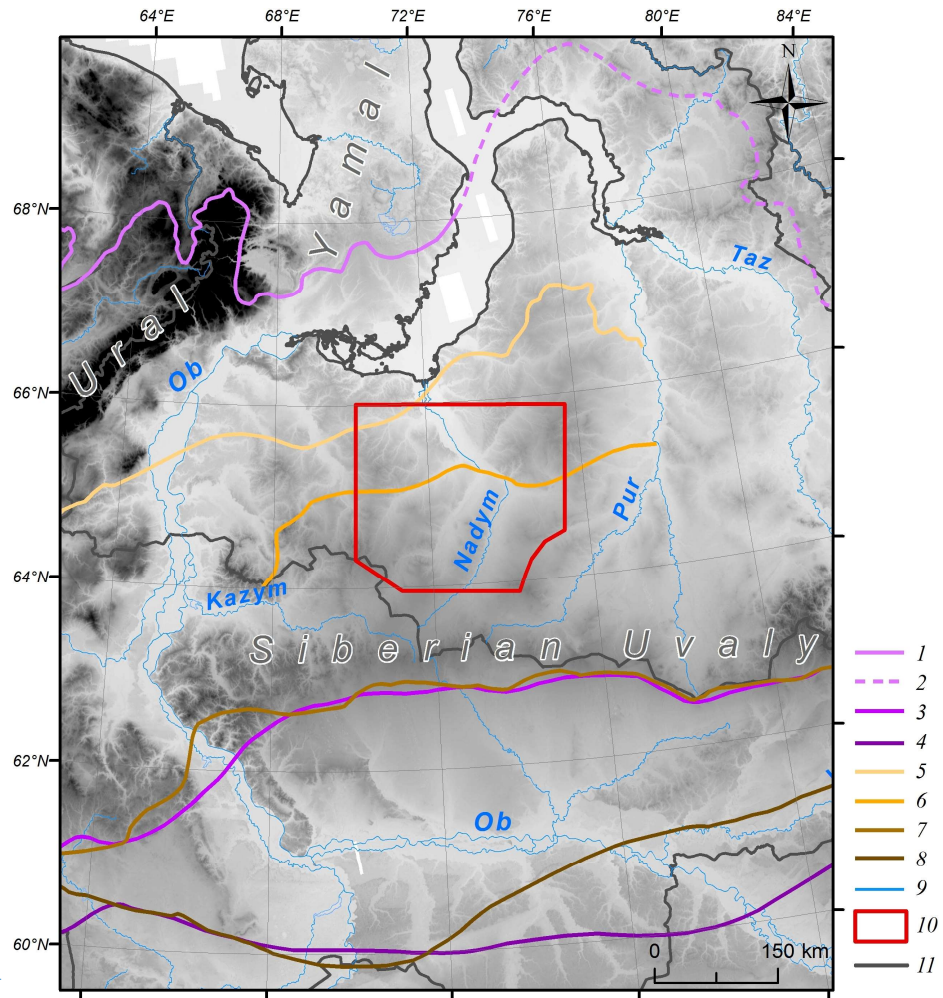
566 *Fig. 12. 1-8: ice sheet boundaries (1: Zyryanka (Astakhov et al., 2016); 2: Zyryanka (assumed)*
567 *(Astakhov et al., 2016); 3: Taz (Astakhov et al., 2016); 4: Samarovo (maximum) (Astakhov et al.,*
568 *2016); 5: Zyryanka (Zemtsov, 1976; Babushkin, 1996); 6: Taz (second stage) (Zemtsov, 1976;*
569 *Babushkin, 1996); 7: Taz (Zemtsov, 1976); 8: Samarovo (Zemtsov, 1976)); 9: water bodies;*
570 *10: study area; 11: administrative boundaries. Background: TanDEM-X 90m DEM ©DLR.*
571

| Age (Ma) | | | East-European Plain | MIS | Western Siberia |
|---|---|---|---|---|---|
| 0 | Holocene | | Holocene | 1 | Holocene |
| | | | Valdai cold | 2 | Sartanian cold |
| | | LATE | warm | 3 | Karginian warm |
| | | | cold | 4 | Ermakovian(Zyrian) cold |
| 0.1 | | | Mikulino warm | 5 | Kazantsevo warm |
| | PLEISTOCENE | | Dnieper (Moscow) cold | 6 | Tazovian cold |
| 0.2 | | MIDDLE | Cherepet warm' | 7 | Shirta warm |
| | | | Zhizdra cold | 8 | Samarovo cold |
| 0.3 | | | Chekalin warm | 9 | Tobolian warm |
| | | | Kaluga cold | 10 | |
| 0.4 | | | Likhvin warm | 11 | |

572
573 *Fig. 13. Palaeoenvironmental event successions on the East-European Plain (from*
574 *Bolikhovskaya, 2004; Molodkov and Bolikhovskaya, 2010) and in Western Siberia (Interregional*
575 *Stratigraphic Chart..., 2014).*
576

The key natural feature of the glacial genesis of Quaternary strata in northern Western Siberia is the presence of wrecked rock: semi-rounded angular stones, gravel and large boulders with evident glacial striation, carried over by the glacier from the territories outside the West Siberian Plain (Strelkov et al., 1965; Zemtsov, 1976). The water-glacial sediments in the research area include well-washed grey sand characterized by poor chemical composition (the gravimetric concentration of $SiO_2$ is 94-97%) and also containing amendments of gravel and stones (Chekunova, 1954; Groysman, 1954; Khlebnikov, 1954). The glacial sediments include unsorted coarse-grained sands with an abundance of pebbles, as well as moraine-like bodies of lumped clay, loam, and clay sand with gravel and large boulders. The petrographic composition of boulders and pebbles includes quartz, opal, sandstones, quartz porphyres, amphibolites, granitoids, gneises and trachites (Chekunova, 1954; Groysman, 1954; Khlebnikov, 1954). However, it was noted that interpreting the exact location of the origin of these rocks from the geological markers representing different territories is so far problematic.

The results of the study of the sections, in general, showed that the youngest of the discussed sediments are those of the second floodplain terrace (section NS-6, K-1). In the top part, it includes aeolian sand formed no later than the beginning of the Holocene (MIS 1), in the middle part there are floodplain series of alluvium, in the lower part there are river streams of grey oblique sand of the late MIS 3 – middle MIS 2.

The absolute age of the second floodplain terrace formation of the Nadym and Tanlova Rivers (sections K-1 and NS-6) correlates well with radiocarbon and OSL datings of postglacial Pleistocene sediments throughout all the northern Western Siberia (the age ranging from 42,000 to 25,000 years) (Astakhov and Nazarov, 2010). On average, the age of the cover formation is between 20,000 and 12,000 years (Astakhov, 2006; Zemtsov, 1976) Two types of glacial relief areas and extensive sandur surfaces were identified on the surface of the second floodplain terrace in the large-scale field studies on the left bank of the Left Kheta River (Vasilyev, 2007).

On the middle and upper topographical level, grey monoquartz sand in sections NS-20 and NS-22 was also found. Its age is similar: the beginning of MIS5. It can be suggested that during the Kazantsev interglacial period in the vast area of the Nadym River basin there were favorable conditions for the erosion of the previously accumulated sandy textured deposits and their transfer downstream the main rivers.

One of the most interesting points of research is the kameform hill on the left bank of the Right Khetta River (NS-13/14), the formation of its middle part corresponds to the Tobol interglacial period (MIS 9-11). It can be suggested that the sediments in the upper part of the hill are not younger than the Taz glaciation (MIS 6), while the pebble layer formed during the degradation of the glacier reinforced the previous sediments and later was resistant to erosion, and was not covered by the waters of the Kazantsev and Karga transgressions

The results of the sand quartz grain morphology analysis confirmed the supposed genesis of the studied sections. Thus, for sections NS-6 and K-1 it was

shown that in the upper part of sections the sequence is: aeolian sediments, aluvial flood plain facies, and channel facies of coarse stratified sands. At the base of both sections, there are sediments in which, apart from typically river grains, a large number of various morphology grains are found. These are grains of varying degree of roundness, irregular shape with a smooth surface and smooth faces, often on their surface, there are various grooves and scratches formed under the strong mechanical impact, as well as conchoidal fractures. Their origin could be a result of freezing weathering and cryogenic transformation (Velichko and Timireva, 1995), as well as of high pressure applied to the grain surface (Immonen et al., 2014; Vos et al., 2014). Well-rounded ellipsoid and ball-shaped grains predominate in the top layer sediments. One can associate this distribution with materials coming from two different sources. One source could have been the former glacial sediments eroded by fluvial processes. This type of terrace structure corresponds well with the results of the study by Velichko et al. (2011) who analyzed sands with underlay peat deposits in the investigated region.

Quartz grains from sections NS-13/14 and NS-20 are often characterized by low rounding classes, multiple conchoidal fractures, sometimes even conchoidal systems, a deep-pitted surface, scratches, grooves, and cleavage surfaces. Such elements could be signs of processes that occur in glacial environments. Often, there are also signs of subsequent water treatment: separate crescentic depressions and smoothed sharp peaks of grains. It indicates the redeposition of the glacial grains by water flows. Along with the grains described above, there are also typical subaquatic grains: well-rounded with a fine-pitted surface, but their number is inferior to grains with glacial features.

Currently, we lack sufficient evidence to confirm the glacial genesis of these deposits. It is possible that the grains were exposed to the effects of glacial processes, with a final processing phase in their history that included subaquatic processes. In section NS-22, the grain morphology provides evidence that suggests the existence of a quiet subaquatic environment under which quartz grains underwent long-term treatment.

In general, the results of sand quartz grain morphoscopy and morphometry show that most quartz grains from all sections underwent complex multi-stage processing throughout their life.

The petrographic diversity of erratic boulders in West Siberia helps us distinguish two or three paleoglacial regions that combine several dozen distributed provinces. Each is characterized by a specific set of rocks and petrographic features. The first major generalization in this respect was made by Zemtsov (1976), who identified the guide boulders of the Ural region as ultramafic and mafic rocks of the Main (axial) Uralian zone, plagio-granites, and highly metamorphosed rocks (gneisses and shales). In the Central Siberian region, the prevailing boulders include dolerites and basalts of the Putorana Plateau, as well as various granitoids, quartzites, and Palaeozoic sandstones of the Taimyr Region. These studies were substantially supplemented and detailed work by Sukhorukova et al. (1987).

Despite their small quantity, the petrographic analysis of pebbles and boulders led to the following conclusions. First, high-silica alkaline effusive rocks (sample

667 N-10, quartz trachyte) are indicative of both the Northern Taimyr Province (Troitsky
668 and Shumilova, 1973) and many moraines of the Ural paleoglacial region
669 (Sukhorukova et al., 1987), but they are never found in the Putorana Plateau and the
670 southmost regions. Moreover, there is only a small relative share of dolerites (sample
671 N-14, dolerite) and other effusive mafic rocks, which is a property of Putorana and
672 Nizhnyaya Tunguska regions. In contrast, there is no limestone that would be typical
673 of the Central Siberian paleoglacial region (Kulyumbinsk and Sukhaya Tunguska
674 distributive provinces according to Sukhorukova et al., 1987). There is no granite in
675 the samples either, which is a property of the Northern Taimyr region.

676 Second, quartz and quartzite sandstones are typical for the Ural paleoglacial
677 region, but their share is usually within a few per cent. Quartzitic sandstones also
678 described as Palaeozoic were found 50 km north of Surgut within the tentative
679 Central Siberian and Middle rock outwash zones (Sukhorukova et al., 1987). The
680 source of the polymictic platy jointing sandstone could be the Palaeozoic bordering
681 of the eastern slope of the Urals (Sukhorukova et al., 1987) or the Mesozoic
682 sandstone of the West Siberian Plate.

683 In general, the samples have a significant proportion of terrigenous rocks
684 (sandstones and siltstones) and low content of dolerites. On the one hand, this can
685 be explained by the poor representativeness of the samples. Nevertheless, the key
686 washout zone could be located further north than the Putorana Plateau in the Taimyr
687 area. To substantiate this point of view, further research is planned to determine the
688 trace element composition and absolute dating and to expand the sampling.

689 Despite the numerous features that make it possible to attribute the thickness
690 of grey monomineral quartz sand (K-1, NS-6, NS-20) to fluvioglacial sediments, and
691 the upper pebble strata of section NS-13/14 to glacial sediments, the study did not
692 find typical moraine-like formations of lumped clay, loam and clay sand with gravel
693 and large boulders in this territory. However, detailed descriptions of this type of
694 sediment can be found in some references (Strelkov S.A. et al., 1965; Zemtsov,
695 1976; Sukhorukova et al., 1987; Babushkin, 1996 etc.).

696 Thus, in the middle course of the Right Khetta River at Point 70 (Khlebnikov,
697 1954) 2.5 m deep there is a 20 m-thick until of densely clumped loam with
698 interlayers of mica enriched sand (the layers are up to 25 cm thick) (section AS-1,
699 Figure 9). The color of the loam is brown, small glitter mica is visible, and angular
700 debris (granite) are found, up to 25 cm in diameter. In the right part of the section
701 upstream, stripping exposed a layer of fine-grained sand. Below 15 m it is followed
702 by an interlayer of gravel-pebble rock. The prominent colluvium slope is covered by
703 loam crushed stone, and a cluster of gravel-pebble rock is also found on the towpath.

704 The huge kame moraine was described in the watershed of Nadym and Left
705 Khetta rivers (point 2368) (section AS-2, Figure 9) (Khlebnikov, 1954). It has a wide
706 extension and rises up to 25-30 m above the surrounding plain. The ridge part of the
707 range is convex and consists of individual peaks separated by meso ridges. On the
708 surface of the ridge, the congestion of pebble and gravel is found. The gravel-pebble
709 coarse-grained well-washed and leached sand is traced down to the depth of 1.2 m.

710 Two esker-like linear elevations and a small kameform hill were discovered
711 in the lower course of the Right Khetta River at well No. 18 (Khlebnikov, 1954) at

1.8 m depth in the gravel-pebble horizon with a total depth of 17.6 m (section AS-3, Figure 9). The diameters of the pebbles are between 0.5 and 3-4 cm. The pebbles are not rounded and consist mainly of quartz and sandstone.

The moraine hills in the upper part of the Big Huhu River (right tributary of the Nadym River) have a north-west and a north-east orientation. The length reaches 6-7 km, and the relative height varies from 15 to 60 m. (Chekunova, 1954; Yevseyev, 1958) morphologically, the steep slopes of the hills have individual smoothed tops separated by small saddles. The upper layer of the hills to a depth of 1-2 m is peeled loam with abundant pebble rock. The pebbles are weak and poorly rounded, and their diameters do not exceed 2-4 cm. Petrographic composition in one of the sections reveals (so-called point 367 (Chekunova, 1954)): silica, clay shale, arkoses sandstones, breccia of clay-quartz rocks and limonite. The results of manual drilling at some small hills (Yevseyev, 1958; Andreev, 1960) showed that they are folded with permafrost sediments. The total ice content as determined visually is not less than 30%. As an example, well No. 10 (Yevseyev, 1958), where light grey clay with yellowish color, light, porous, with alevrite interlayers is found at a depth of 1.4-10.7 m, has a wavy and horizontal lamination (section AS-4, Figure 9). Clay thickness is underlayed with grey clay fine-grained sands with poor sorting and admixture of gravel grains, quartz, and silicon pebbles.

Data from both our studies and previous field studies are in good correspondence to the results of the analyses with the Tandem-X Digital Terrain Models. These models revealed that despite the plain origin of the territory, the high salinity and dominance of erosion processes, various glacial and fluvioglacial relief features preserved to various degrees (kameform hills, proximal moraines, and linear elevations, glacial meltwaters etc.) are evident.

A linear-oriented relief caused by a glacial impact in northern Western Siberia is highlighted on the Map of Quaternary Formations in Russia, 1:2,500,000 scale (Astakhov et al., 2016). At the same time, linear features and glacial remains are identified on geological maps of larger scales (Babushkin, 1996).

Nowadays, due to the increasing availability of initial DTM data, remote mapping of glacial relief features become the standard method across the world (Clark et al. 2004; Glasser et al. 2008; Sharpe et al. 2010; Atkinson et al. 2014; Norris et al. 2017). Based on modern spatial data, a detailed map for the British Isles Territory and Coastal Zone (BRITICE-2) is available for digital study and analysis, and was updated (Clark et al., 2018). The remote features of most forms of glacial relief for various natural conditions are described in detail and offer numerous evidence that can be used as standards for remote sensing data interpretation, including the entire north area of Western Siberia.

### *Conclusions*

Our results showed high efficiency of simultaneous application of field ground and remote methods even with limited raw site rocks. Sediments were identified, which can be immediately attributed to fluvioglacial (lower part of section K-1 and NS-6, section NS-20) and glacial (upper layer of section NS-13/14) origins. Traces of glacial treatment were also found as landforms in certain areas

such as kameform hills, proximal moraines, linear-bed elevations, and depressions of melt glacial water runoffs. Due to low organic substance content, sparse lichen-pine trees are formed over the fluvioglacial sediments on the low-fertile podzolic soils. It is a characteristic landscape feature of the leaching soil condition for the north taiga in Western Siberia. At the same time, the moraine-like layers of aggregated clay, loam and clay sand with gravel and large boulders that could not be found in field studies are widely described in sources previously unpublished (particularly the Left Khetta and in the upper reaches of the Big Huhu River).

Thus, the development history of the Nadym River lower stream area provides evidence that periods of cover glaciations occurred here in the Pleistocene. At the same time, it is difficult to say whether it was a single glacier with a common front, or whether there were several separate centers of ice accumulation. The available data, especially the structure and functional characteristics of the relief, appear to favor the second option, at least in the late Pleistocene. In the early periods, traces of larger glaciation may represent the vast lake-alluvial plains and flood plains, reaching a maximum area in the basin of the Nadym, Pur and Taz rivers. In this case, they can be considered as the latest erosion formations but preserved a characteristic structure inherited by modern landscapes.

### *Acknowledgements*

The authors thank the Terrasar-X (DLR) research team for providing the TanDEM DTM for research (DEM_GEOL1378). We also thank the anonymous reviewers whose comments and suggestions helped improve and clarify this manuscript.

This study was funded by the RFBR and the Yamal-Nenets Autonomous District, project number 19-45-890008. The investigation is under a public assignment by the Institute of Geology and Mineralogy, SB, RAS.

### *References*

Alyavdin F.A., and Mokin N.P.: Geological map. 1rd ed. Scale 1:1,000,000. Ministry of Geology and Subsoil Protection of the USSR, Map Q-43 (Novyy Port). Gosgeoltekhizdat, Moscow, 1957.

Andreev Yu.F.: About the relationship of linear-ridge topography with tectonic structures in the north of Western Siberia (in the field of permafrost development). Geologiya i geokhimiya. Geology and geochemistry, 3(IX), 76–94, 1960.

Astakhov, V.I.: On chronostratigraphic units of the Upper Pleistocene in Siberia, Geologiya i geofizika, 47(11), 1207–1220, 2006.

Astakhov, V., and Nazarov, D.: Correlation of Upper Pleistocene sediments in northern West Siberia. Quaternary Science Reviews, 29(25-26), 3615–3629., 2010.

Astakhov, V., Shkatova, V., Zastrozhnov, A. and Chuyko, M.: Glacio-morphological Map of the Russian Federation, Quaternary International, 420, 4–14, 2016.

Atkinson, N., Utting, D., and Pawley, S.: Landform signature of the Laurentide and Cordilleran ice sheets across Alberta during the last glaciation. Canadian Journal of Earth Sciences, 51(12), 1067-1083, doi: 10.1139/cjes-2014-0112, 2014

Babushkin, A.E.: Quaternary map. 2rd ed. Scale 1:1,000,000. Russian Federation Committee on Geology and Mining (Roskomnedra), Map Q-42,43 (Salekhard). St. Petersburg: VSEGEI Cartographic Factory, 1996.

804    Bolshiyanov, D.Yu.: Passive Glaciation of the Arctic and Antarctic Regions. AANII, Saint
805           Petersburg, 296 p, 2006.
806    Chekunova, V.S.: Geological and geomorphological survey of a part of the lower reaches of the
807           Nadym River basin and parts of the right bank of the Nadym Ob River. VSEGEI, Leningrad,
808           1954.
809    Clark, C, Evans, D, Khatwa, A., Bradwell, T., Jordan, C., Marsh, S., Mitchell, W. and Bateman,
810           M.: Map and GIS database of glacial landforms and features related to the last British ice
811           sheet. Boreas, 33, 359–375, 2004.
812    Clark, C., Ely, J., Greenwood, S., Hughes, A., Meehan, R., Barr, I., Bateman, M., Bradwell, T.,
813           Doole, J., Evans, D., Jordan, C., Monteys, X., Pellicer, X.. and Sheehy, M.: BRITICE Glacial
814           Map, version 2: a map and GIS database of glacial landforms of the last British–Irish Ice
815           Sheet. Boreas, 47, 11–27, 2018.
816    Bolikhovskaya, N.S.: Paleoenvironments and climato-stratigraphy of the loess-paleosol formation
817           of Northern Eurasia. Loess inForm, 4, 11–36, 2004.
818    Faibusovich, Ya.E. and Abakumova, L.A.: Map of Pliocene-Quaternary formations. 3rd ed. Scale
819           1:1,000,000. Federal Agency for Subsoil Use (Rosnedra), Map Q-43 (New Urengoy). St.
820           Petersburg: VSEGEI Cartographic Factory, 2015.
821    Fredin, O., Rubensdotter L., Welden, A., Larsen, E. and Lysa, A.: Distribution of ice marginal
822           moraines in NW Russian, Journal of Maps, 8(3), 236–241, 2012. doi:
823           10.1080/17445647.2012.708536
824    Glasser, N., Jansson, K., Harrison, S., and Kleman, J.: The glacial geology and Pleistocene history
825           of South America between 38,8S and 56,8S. Quaternary Science Reviews, 27, 365–390,
826           2008.
827    Grosvald, M.G.: Eurasian Hydrospheric Catastrophes and Glaciations of the Arctic Region,
828           Nauchny Mir, Moscow, 1999.
829    Groysman, Ya.M.: Geological survey of the Haigi-Yakh River basin (Long-Yugan). VSEGEI,
830           Leningrad, 1954.
831    Generalov, P.P.: Upper Pleistocene of the lower course of the Ob River In: Collection of scientific
832           papers of the West Siberian Scientific and Research Geological Prospecting Petroleum
833           Institute, Tyumen, 56–77, 1986.
834    Immonen, N., Strand, K., Huusko, A., and Lunkka, J.P.: Imprint of late Pleistocene continental
835           processes visible in ice-rafted grains from the central Arctic ocean. Quaternary Science
836           Reviews 92, 133–139, 2014.
837    Interregional stratigraphic chart of the Quaternary of the territory of the Russian Federation.
838           Interdepartmental Stratigraphic Committee, VSEGEI, St. Petersburg, 2014.
839    Kalinska-Nartisa E., Woronko B., and Ning W.: Microtextural inheritance on quartz sand grains
840           from Pleitocene periglacial environments of the Mazovian Lowland, Central Poland.
841           Permafrost and Periglacial Processes 28, 741–756, 2017.
842    Khabakov, A.V.: On roundness indexes of pebble, Sovetskaya Geologiya, 10, 98–99, 1946.
843    Khlebnikov, V.I.: Geological and geomorphological survey of a part of the middle reaches of the
844           Nadym river basin. VSEGEI, Leningrad, 1954.
845    Krinsley, D.H., and Doornkamp, J.C.: Atlas of quartz sand surface textures. 2nd edition.
846           Cambridge, Cambridge University Press, 102, 2011.
847    Kind, N.V.: Late Quaternary Geochronology According to Isotope Data. Nauka, Moscow, 1974.
848    Lazukov, G.I.: Antopogen of the northern part of Western Siberia (Paleogeorgaphy), Moscow, 127
849           p, 1972.
850    Maslennikov, V.V.: Regional Geo-Ecological Mapping at Scale of 1:1000000 Within the North
851           End of Tyumen Oblast. Labytnangi, 1998.
852    Molodkov, A.: The Late Pleistocene palaeoenvironmental evolution in Northern Eurasia through
853           the prism of the mollusc shell-based ESR dating evidence. Quaternary International, (in
854           press.), 2020.

855  Molodkov, A.: Cross-check of the dating results obtained by ESR and IR-OSL methods:
856      implication for the Pleistocene palaeoenvironmental reconstructions. Quat. Geochronol., 10,
857      188–194, 2012.
858  Molodkov, A., and Bolikhovskaya, N.: Climato-chronostratigraphic framework of Pleistocene
859      terrestrial and marine deposits of Northern Eurasia based on pollen, electron spin resonance,
860      and infrared optically stimulated luminescence analyses. Est. J.Earth Sci. 59(1), 49–62,
861      2010.
862  Molodkov, A., and Bitinas, A.: Sedimentary record and luminescence chronology of the
863      Lateglacial and Holocene aeolian sediments in Lithuania. Boreas, 35 (2), 244–254, 2006.
864  Norris, S. L., Margold, M., and Froese, D.G.: Glacial landforms of northwest Saskatchewan.
865      Journal of Maps, 13, 600–607, doi:10.1080/17445647.2017.1342212, 2017.
866  Rukhin, L.B.: Fundamentals of Lithology. Doctrine of Sedimentary Rocks. Nedra, Leningrad,
867      1969.
868  Rusakov, A., Sedov, S., Sheinkman, V., Dobrynin, D., Zinovyev, E., Trofimova, S. and
869      Levchenko, S.: Late Pleistocene paleosols in the extra-glacial regions of Northwestern
870      Eurasia: Pedogenesis, post-pedogenic transformation, paleoenvironmental inferences.
871      Quaternary International. 501, 174-192, doi:10.1016/j.quaint.2018.03.020, 2018.
872  Sharpe, J., Sharpe, D., and Harris J.: A flowline map of glaciated Canada based on remote sensing
873      data. Canadian Journal of Earth Sciences, 47, 89–101, 2010.
874  Sedov, S., Rusakov, A., Sheinkman, V., and Korkka, M.: MIS3 paleosols in the center-north of
875      Eastern Europe and Western Siberia: Reductomorphic pedogenesis conditioned by
876      permafrost? Catena, 146, 38–47, doi:10.1016/j.catena.2016.03.022, 2016
877  Sheinkman, V., Sedov, S., Shumilovskikh, L., Korkina, E., Korkin, S., Zinovyev, E. and Golyeva,
878      A.: First results from the Late Pleistocene paleosols in northern Western Siberia:
879      Implications for pedogenesis and landscape evolution at the end of MIS3. Quaternary
880      International, 418, 132–146, doi:10.1016/j.quaint.2015.12.095, 2016.
881  Sizikova, A.O. and Zykina V.S.: The dynamics of the Late Pleistocene loess formation, Lozhok
882      section, Ob loess Plateau, SW Siberia. Quaternary International, 365, 4–14, 2015.
883  Strelkov S.A., Saks V.N., Arkhipov S.A., and Volkova V.S.: The problem of the Quaternary
884      glaciations of Siberia. The main problems of the study of the Quaternary period, Nauka,
885      Moscow, 188–205, 1965.
886  Svendsen, J., Alexahderson, H., Astakhov, V., Demidov, I., Dowdeswell, Ju., Funder, S., Gataulin,
887      V., Henriksen, M., Hjort,H., Houmark-Nielsen, M., Hubberten, H.-W., Ingolfsson,
888      O.,Jakobsson, M., Kjar, K., Larsen, E., Lokrantz, H., Lunkka, Ju. P.,Lysa, A., Mangerud, J.,
889      Matiouchkov, A., Murray, A., Moller, P., Niessen, F., Nikolskaya, O., Polyak, L., Saarnisto,
890      M., Siegert, Ch., Siegert, M., Spielhagen, R. and Stein, R.: Late Quaternary ice sheet history
891      of Northern Eurasia. Quaternary Science Reviews, 23 (11-13), 1229–1271, 2004.
892  Sukhorukova, S.S., Kostyuk M.A., Podsosova, L.L., Babushkon A.E., Zolnikov, I.D., Abramova,
893      S.A. and Goncharov, S.V.: Moraines and Dynamics of Glaciation in Western Siberia. Works
894      of Institute of Geology and Geochemistry of the Siberian Branch of the USSR Academy of
895      Sciences, Issue 672. Nauka, Novosibirsk, 1987.
896  Troitskiy, S.L. and Shumilova, E.V.: Stratigraphy and Mineralogical-Petrographic Peculiarities of
897      Quaternary Deposits in the Vorontsov Yar Stratum in the Lower Course of the Yenisei River.
898      In: Lithology and Conditions of Formation of the Quaternary Deposits of the Northern
899      Eurasia, Institute of Geology and Geochemistry of the Siberian Branch of the USSR
900      Academy of Sciences, Novosibirsk, 5–37, 1974.
901  Vasilyev, S.V.: Forest and Bog Landscapes of Western Siberia. Izdatelstvo NTL, Tomsk, 2007.
902  Velichko, A.A. and Timireva S.N.: Morphoscopy and morphometry of quartz grains from loess
903      and buried soil layers, GeoJournal, 36(2/3), 143–149, 1995.
904  Velichko, A.A., Timireva, S.N., Kremenetski, K.V., McDonald, G.M. and Smith, L.C.: West
905      Siberian Plain as a late glacial desert, Quaternary International, 237 (1-2), 45–53, 2011.
906  Velichko, A.A.: Current state of conceptions on continental glaciers of the Earth. Bulletin of the

907                  Academy of Sciences of the USSR, Geographical Series, 3, 21–34, 1987.

908 Velichko, A.A., Konononv, V.M. and Faustova M.A.: The last glaciation of Earth: size and volume

909                  of ice-sheets, Quaternary International, 41 (42), 43–51, 1997.

910 Vos, K., Vandenberghe, N. and Elesen, J.: Surface textural analysis of quartz grains by scanning

911                  electron microscopy (SEM): From sample preparation to environmental interpretation,

912                  Earth-Science Reviews, 128, 93–104, 2014.

913 Woronko, B.: Frost weathering versus glacial grinding in the micromorphology of quartz sand

914                  grains: Process and geological implications. Sedimentary Geology, 335, 103–119, 2016.

915 Zemtsov, A.A.: Geomorphology of the West Siberian Plain (Northern and Central Parts),

916                  Publishing house of the Tomsk State University, Tomsk, 1976.

917 Yevseyev, G.P., and Reynin, I.V.: Geological structure and geomorphology of the Tanlova, Right

918                  Khetta, and Big Huhu basins (right tributaries of the middle segment of the Nadym river).

919                  VNIGRI, Leningrad, 1958.

920

921 ***Annexes***

922

923 Annex 1. Bulk content of chemical elements

| Sampling depth, m | Sample No | Bulk content, % | | | | | | | |
|---|---|---|---|---|---|---|---|---|---|
| | | SiO$_2$ | Al$_2$O$_3$ | Fe$_2$O$_3$ | K$_2$O | Na$_2$O | P$_2$O$_5$ | CaO | TiO$_2$ |
| К-1 | | | | | | | | | |
| 0.1 | S1 | 87.65 | 5.27 | 0.95 | 1.66 | 1.00 | 0.03 | 0.51 | 0.64 |
| 0.35 | S2 | 88.09 | 5.14 | 1.89 | 1.14 | 0.56 | 0.05 | 0.32 | 0.53 |
| 1 | S3 | 89.49 | 4.93 | 1.20 | 1.52 | 0.75 | 0.04 | 0.41 | 0.41 |
| 1.8 | S4 | 92.97 | 3.35 | 0.61 | 1.32 | 0.51 | 0.02 | 0.27 | 0.21 |
| 2.3 | S5 | 90.71 | 4.21 | 0.92 | 1.35 | 0.64 | 0.03 | 0.38 | 0.39 |
| 3 | S6 | 98.02 | 0.88 | 0.30 | 0.25 | 0.07 | 0.01 | 0.10 | 0.10 |
| 4 | S7 | 98.39 | 0.69 | 0.25 | 0.20 | <0.05 | 0.01 | 0.08 | 0.08 |
| NS-6 | | | | | | | | | |
| 0.3 | S1 | 90.60 | 6.20 | 0.87 | 0.91 | 0.63 | 0.08 | 0.28 | 0.37 |
| 0.7 | S2 | 91.85 | 4.57 | 0.74 | 1.47 | 0.58 | 0.01 | 0.41 | 0.37 |
| 1.4 | S3 | 93.22 | 3.92 | 0.51 | 1.15 | 0.57 | 0.01 | 0.31 | 0.25 |
| 3.2 | S4 | 92.37 | 4.05 | 0.75 | 1.38 | 0.62 | 0.02 | 0.43 | 0.35 |
| 4 | S5 | 90.32 | 5.39 | 0.98 | 1.74 | 0.62 | 0.02 | 0.46 | 0.47 |
| 4.2 | S6 | 97.33 | 1.54 | 0.26 | 0.15 | 0.45 | 0.00 | 0.18 | 0.08 |
| 4.6 | S7 | 89.79 | 5.86 | 0.95 | 1.80 | 0.65 | 0.03 | 0.63 | 0.35 |
| 5 | S8 | 96.65 | 1.88 | 0.28 | 0.42 | 0.49 | 0.01 | 0.20 | 0.11 |
| 7.4 | S9 | 97.29 | 1.46 | 0.24 | 0.25 | 0.48 | 0.01 | 0.16 | 0.07 |
| 9.2 | S10 | 97.78 | 1.19 | 0.21 | 0.07 | 0.45 | 0.01 | 0.17 | 0.07 |
| NS-13/14 | | | | | | | | | |
| 1.1 | S1 | 97.72 | 1.43 | 0.21 | 0.00 | 0.43 | 0.00 | 0.14 | 0.10 |
| 3.1 | S2 | 91.00 | 1.26 | 5.62 | 0.00 | 0.63 | 1.28 | 0.16 | 0.07 |
| 3.5 | S3 | 96.58 | 1.22 | 1.14 | 0.15 | 0.56 | 0.12 | 0.18 | 0.11 |
| 4 | S4 | 98.14 | 0.99 | 0.15 | 0.00 | 0.48 | 0.00 | 0.15 | 0.07 |
| 4.3 | S5 | 96.25 | 1.18 | 1.58 | 0.07 | 0.47 | 0.06 | 0.16 | 0.24 |
| 4.75 | S6 | 92.75 | 1.23 | 5.08 | 0.01 | 0.64 | 0.02 | 0.18 | 0.12 |
| 5 | S7 | 98.34 | 0.89 | 0.17 | 0.00 | 0.43 | 0.00 | 0.13 | 0.09 |
| NS-20 | | | | | | | | | |
| 1.5 | S1 | 95.61 | 1.79 | 0.39 | 0.48 | 0.08 | 0.02 | 0.08 | 0.44 |
| 3.7 | S2 | 95.59 | 1.83 | 0.21 | 0.68 | 0.09 | 0.01 | 0.07 | 0.16 |
| 6.5 | S3 | 97.12 | 1.14 | 0.19 | 0.39 | 0.09 | 0.01 | 0.07 | 0.10 |
| 9.5 | S4 | 94.30 | 2.31 | 0.31 | 0.84 | 0.10 | 0.02 | 0.07 | 0.38 |
| 16.45 | S5 | 97.26 | 0.93 | 0.22 | 0.22 | 0.05 | 0.01 | 0.07 | 0.20 |
| NS-22 | | | | | | | | | |
| 1.1 | S1 | 96.49 | 1.53 | 0.32 | 0.61 | 0.17 | 0.01 | 0.11 | 0.17 |

924

925

926    Annex 2

927    Spearman's coefficients of correlation

| | $SiO_2$ | $TiO_2$ | $Al_2O_3$ | $Fe_2O_3$ | MnO | MgO | CaO | $Na_2O$ | $K_2O$ | $P_2O_5$ | BaO |
|---|---|---|---|---|---|---|---|---|---|---|---|
| $SiO_2$ | 1 | -1 | -1 | -0.89 | -0.84 | -0.76 | -0.89 | -0.89 | -0.79 | -0.81 | -0.62 |
| $TiO_2$ | -1 | 1 | 1 | 0.89 | 0.94 | 0.75 | 0.89 | 0.89 | 0.79 | 0.83 | 0.73 |
| $Al_2O_3$ | -1 | 1 | 1 | 0.89 | 0.94 | 0.78 | 0.89 | 0.89 | 0.79 | 0.84 | 0.73 |
| $Fe_2O_3$ | -0.89 | 0.89 | 0.89 | 1 | 0.93 | 0.95 | 0.75 | 0.75 | 0.61 | 0.97 | 0.61 |
| MnO | -0.84 | 0.94 | 0.94 | 0.93 | 1 | 0.86 | 0.85 | 0.85 | 0.76 | 0.91 | 0.78 |
| MgO | -0.76 | 0.78 | 0.78 | 0.95 | 0.86 | 1 | 0.67 | 0.67 | 0.52 | 0.99 | 0.54 |
| CaO | -0.89 | 0.89 | 0.89 | 0.75 | 0.85 | 0.67 | 1 | 1 | 0.96 | 0.71 | 0.91 |
| $Na_2O$ | -0.89 | 0.89 | 0.89 | 0.75 | 0.85 | 0.67 | 1 | 1 | 0.96 | 0.71 | 0.91 |
| $K_2O$ | -0.79 | 0.79 | 0.79 | 0.61 | 0.76 | 0.52 | 0.96 | 0.96 | 1 | 0.56 | 0.96 |
| $P_2O_5$ | -0.81 | 0.83 | 0.84 | 0.97 | 0.91 | 0.99 | 0.71 | 0.71 | 0.56 | 1 | 0.59 |
| BaO | -0.62 | 0.73 | 0.73 | 0.61 | 0.78 | 0.54 | 0.91 | 0.91 | 0.96 | 0.59 | 1 |

928    Significance level $p < 0.05$

929

930

931    Annex 3. Grain size distribution

| Sampling depth | Sample | Fraction size (mm) / Content (%) | | | | | |
|---|---|---|---|---|---|---|---|
| | | Silt and clay | Very fine sand | Fine sand | Medium grained sand | Coarse Sand | Very coarse sand |
| **K-1** | | *<0.09* | *0.125-0.09* | *0.25-0.125* | *0.5-0.25* | *1-0.5* | *>1* |
| 0.1 | S1 | 31.7 | 29.2 | 28.7 | 9.5 | 0.7 | 0.1 |
| 0.35 | S2 | 18.7 | 12.5 | 32.1 | 32.2 | 4.2 | 0.3 |
| 1 | S3 | 18.9 | 32.3 | 35.6 | 11.9 | 1.2 | 0.1 |
| 1.8 | S4 | 5.9 | 20.1 | 56.7 | 16.4 | 0.9 | 0.0 |
| 2.3 | S5 | 5.6 | 13.1 | 59.9 | 19.8 | 1.6 | 0.0 |
| 3 | S6 | 0.6 | 0.4 | 1.8 | 71.5 | 23.7 | 1.9 |
| 4 | S7 | 0.4 | 0.5 | 4.2 | 46.3 | 46.9 | 1.7 |
| **NS-6** | | *<0.075* | *0.10-0.075* | *0.25-0.10* | *0.5-0.25* | *1-0.5* | *>1* |
| 0.3 | S1 | 11.0 | 6.6 | 52.7 | 26.9 | 2.8 | 0.0 |
| 0.7 | S2 | 0.8 | 6.8 | 70.8 | 18.7 | 0.4 | 1.9 |
| 1.4 | S3 | 2.0 | 8.8 | 65.8 | 21.2 | 1.3 | 0.5 |
| 3.2 | S4 | 3.6 | 8.4 | 72.8 | 15.2 | 0.0 | 0.0 |
| 4 | S5 | 29.9 | 14.9 | 50.2 | 5.1 | 0.0 | 0.0 |
| 4.2 | S6 | 2.8 | 0.0 | 29.4 | 61.9 | 5.9 | 0.0 |
| 4.6 | S7 | 26.2 | 21.1 | 51.1 | 1.6 | 0.0 | 0.0 |
| 5 | S8 | 0.0 | 0.0 | 41.1 | 55.0 | 3.9 | 0.0 |
| 7.4 | S9 | 1.1 | 0.1 | 29.2 | 52.1 | 17.4 | 0.0 |
| 9.2 | S10 | 0.5 | 0.0 | 29.4 | 57.5 | 12.6 | 0.0 |
| **NS-13/14** | | *<0.075* | *0.10-0.075* | *0.25-0.10* | *0.5-0.25* | *1-0.5* | *>1* |
| 1.1 | S1 | 0.0 | 0.0 | 0.6 | 37.4 | 58.0 | 4.0 |
| 3.1 | S2 | 8.0 | 0.0 | 0.3 | 36.6 | 54.2 | 0.9 |
| 3.5 | S3 | 5.9 | 0.0 | 10.6 | 59.9 | 23.6 | 0.0 |
| 4 | S4 | 0.0 | 0.0 | 7.1 | 62.9 | 30.0 | 0.0 |
| 4.3 | S5 | 24.4 | 1.2 | 15.3 | 40.9 | 18.0 | 0.1 |
| 4.75 | S6 | 1.9 | 0.0 | 6.5 | 53.5 | 37.5 | 0.6 |
| 5 | S7 | 0.0 | 0.0 | 8.0 | 61.5 | 30.6 | 0.0 |
| **NS-20** | | *<0.09* | *0.125-0.09* | *0.25-0.125* | *0.5-0.25* | *1-0.5* | *>1* |
| 1.5 | S1 | 0.0 | 2.2 | 62.1 | 21.9 | 1.3 | 12.5 |
| 3.7 | S2 | 0.0 | 4.3 | 72.0 | 23.0 | 0.5 | 0.2 |
| 6.5 | S3 | 0.0 | 4.4 | 55.8 | 38.5 | 1.1 | 0.3 |
| 9.5 | S4 | 0.0 | 9.3 | 70.7 | 16.0 | 1.5 | 2.4 |
| 16.45 | S5 | 0.0 | 0.9 | 56.8 | 37.6 | 4.0 | 0.6 |
| **NS-22** | | *<0.09* | *0.125-0.09* | *0.25-0.125* | *0.5-0.25* | *1-0.5* | *>1* |
| 1.1 | S1 | 0.0 | 1.4 | 53.3 | 44.3 | 0.9 | 0.1 |

932
933
934
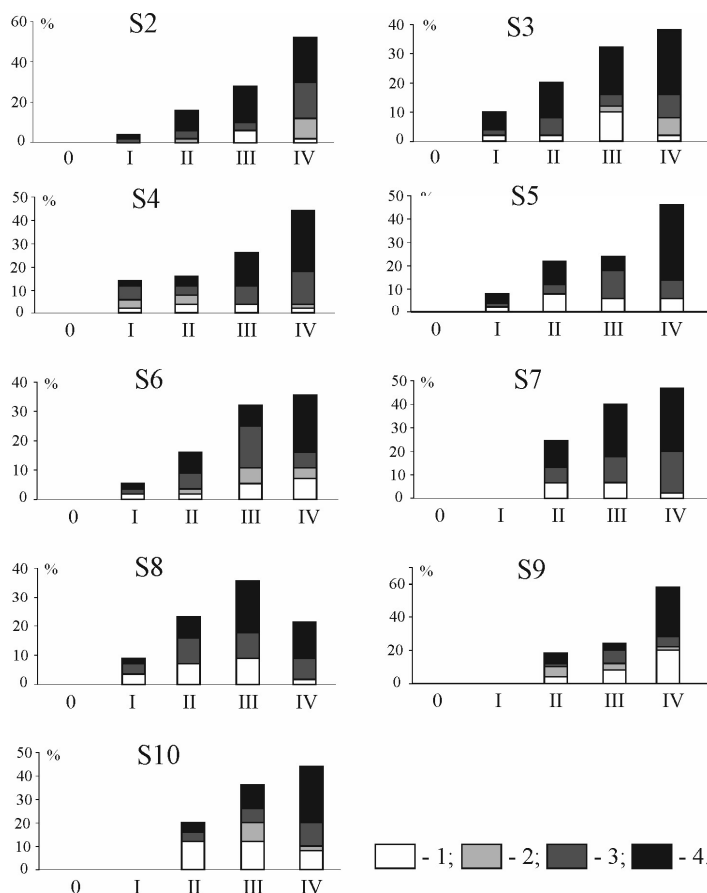
935
936 Annex 4. Distribution of quartz sand grains from section NS-6 by roundness and dullness.
937 1:glossy; 2:quater-matte; 3:half-matte; 4: matte; 0, I, II, III, IV are grades of roundness according
938 to Khabakov (1946) scale.
939
940
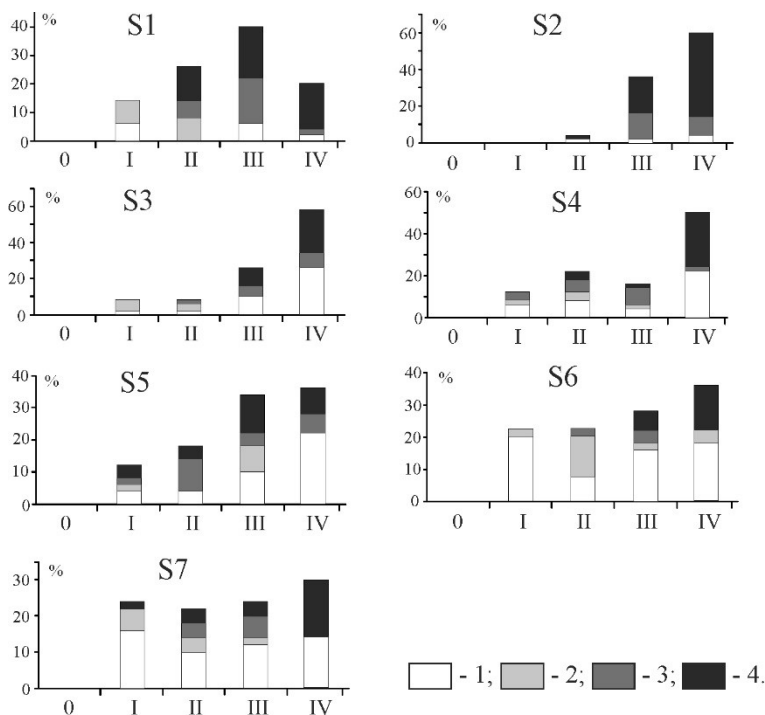
941
942 Annex 5. Distribution of quartz sand grains from section NS-6 by roundness and dullness.
943 1:glossy; 2:quater-matte; 3:half-matte; 4: matte; 0, I, II, III, IV are grades of roundness according
944 to Khabakov (1946) scale.
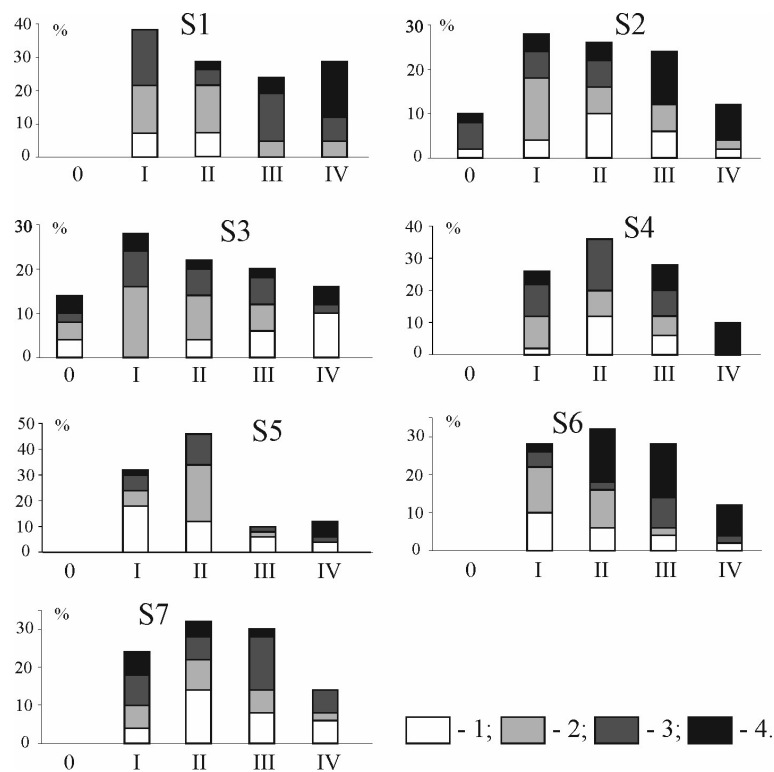
945
946        Annex 6. Distribution of quartz sand grains from section NS-13/14 by roundness and dullness.
947 1:glossy; 2:quater-matte; 3:half-matte; 4: matte; 0, I, II, III, IV are grades of roundness according
948                     to Khabakov (1946) scale.
949
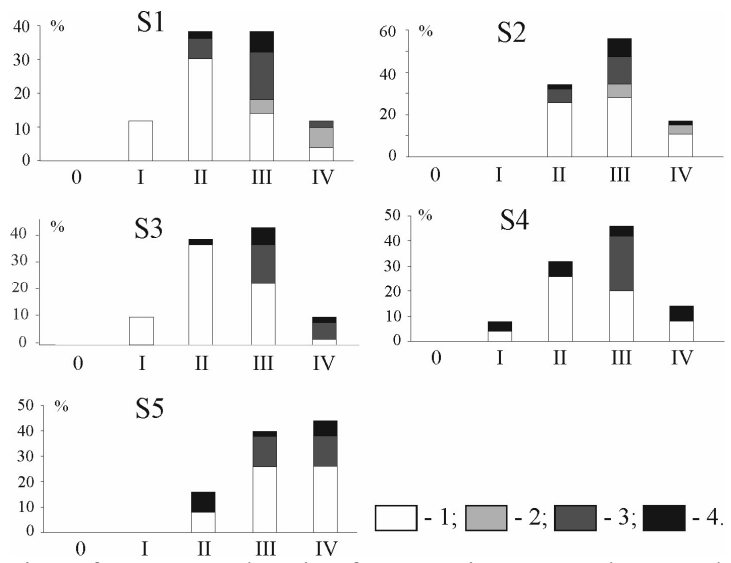
950
951        Annex 7. Distribution of quartz sand grains from section NS-20 by roundness and dullness.
952 1:glossy; 2:quater-matte; 3:half-matte; 4: matte; 0, I, II, III, IV are grades of roundness according
953                     to Khabakov (1946) scale.
954
955
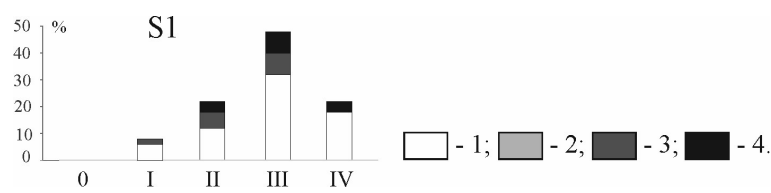
956
957        Annex 8. Distribution of quartz sand grains from section NS-22 by roundness and dullness.
958 1:glossy; 2:quater-matte; 3:half-matte; 4: matte; 0, I, II, III, IV are grades of roundness according
959                     to Khabakov (1946) scale.

960
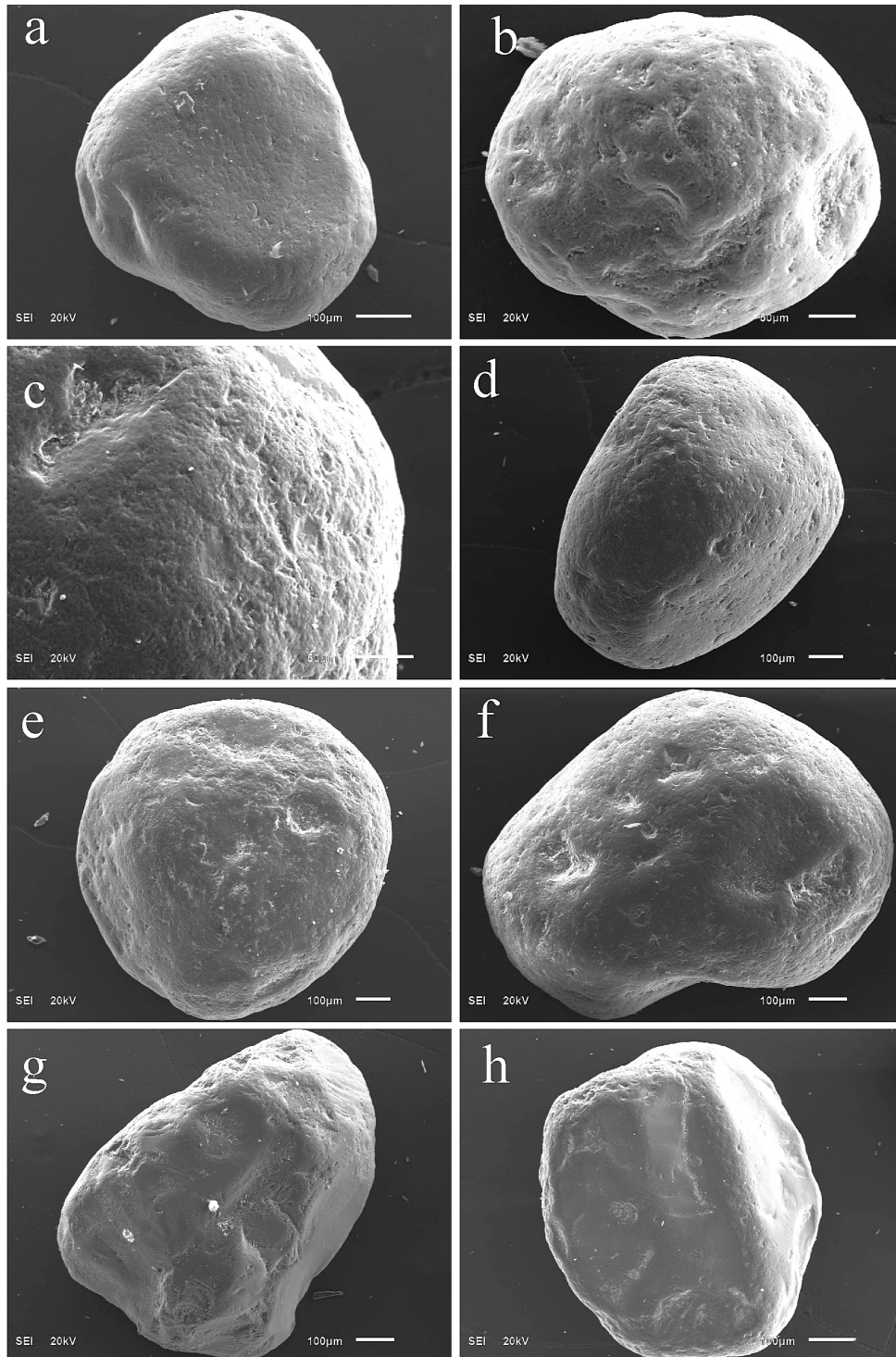
961
962
963 Annex 9. SEM photos of quartz grains, section NS-6.
964 Aeolian sediments: (a): dull grain with a micro-pitted surface and individual crescent-shaped
965 depressions, (b): matte grain with a micro-pitted surface and traces of previous subaquatic
966 treatment.
967 Floodplain sediments: (c): half-matte grain with V-shaped depressions, forming a fine-pitted
968 surface, and with micro-pits, (d): half-matte grain with V-shaped depressions and fine-pitted.
969 Fluvial deposits: (e): glossy grain with a fine-pitted surface; (f): half-matte grain with a fine-pitted
970 surface and separate V-shaped depressions; (g): glossy grain with fine-pits in the protruding parts
971 of the grain; (h): glossy grain with presedimentation fractures, with the surface subjected to aquatic
972 processes, as expressed by the shape of V-shaped depressions.
973

974
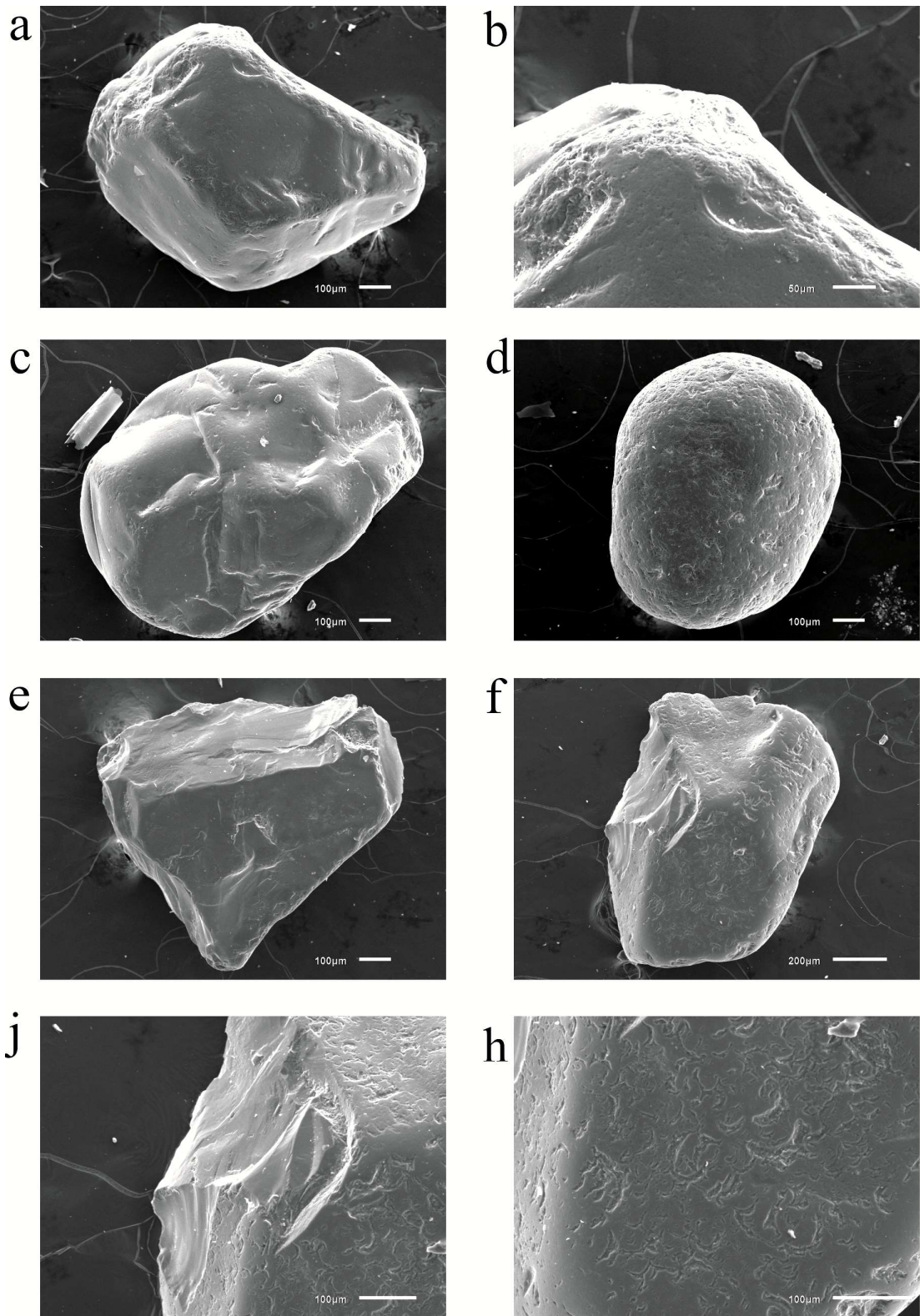
975
976 Annex 10. SEM photos of quartz grains from S7 section K-1: (a): glossy grain with a smooth
977 surface and flat faces; the faces feature crescentic pits, grain tops feature fine pits; (b): fine-pitted
978 surface of grain 'a'; (c): glossy grain with a smooth surface and sparse fine pits; (d): half-matte
979 grain with fine-pitted surface and crescent pits; (e): glossy grain with flat faces and no evident
980 texture; (f): glossy grain with post-sedimentation conchoidal fractures and crescentic pits;
981 (j):conchoidal fracture of grain 'e'; (h): crescentic texture of grain 'e'.
982
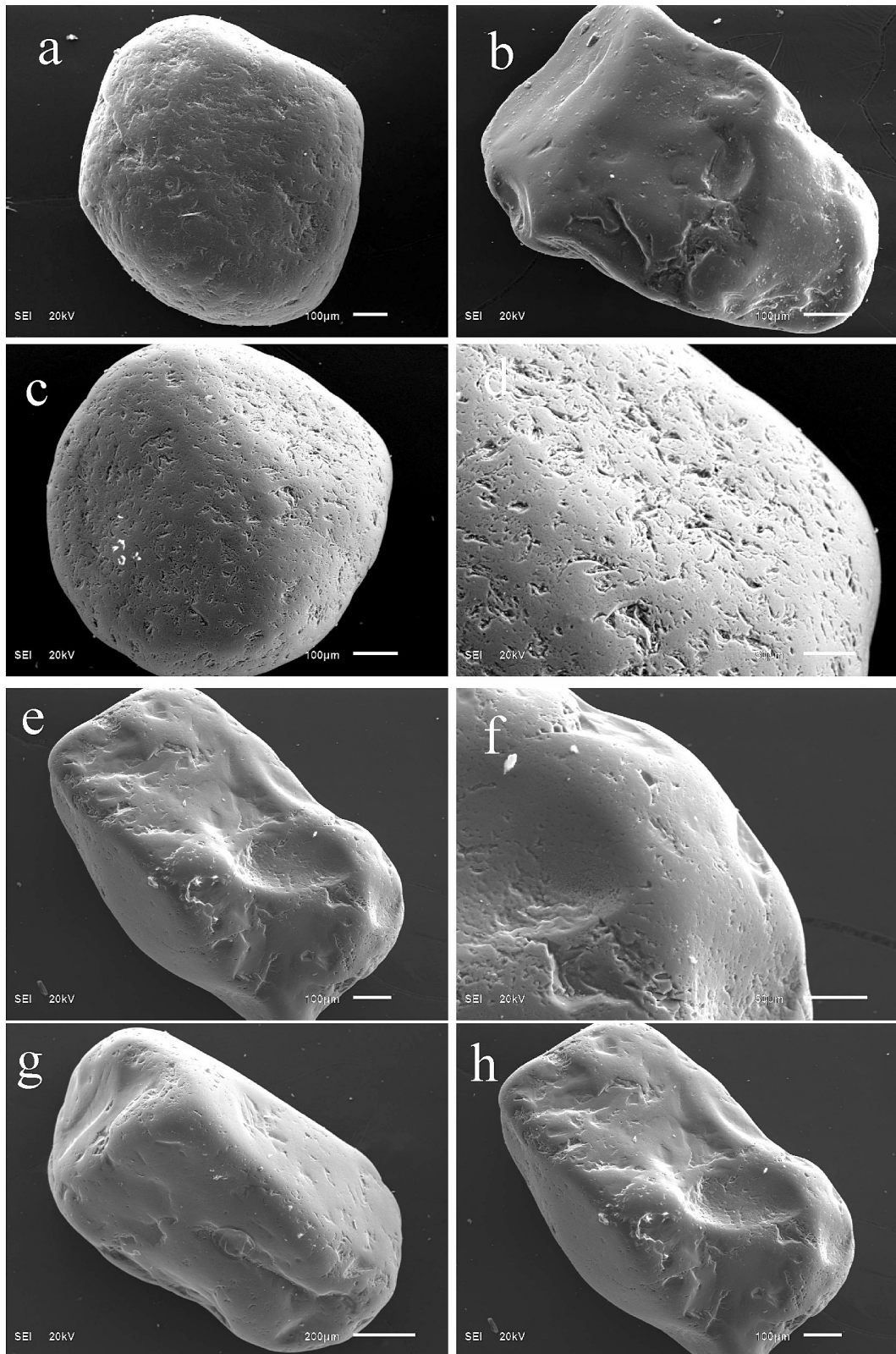
983
984  Annex 11. SEM photos of quartz grains from the section NS-13/14: (a) - glossy grain with fine-
985  pitted and crescent and V-depressions; (b): glossy grain of irregular shape with chips and
986  separate V-shaped recesses; (c), (d): half-matte grain with a crescentic texture and micropits; (e),
987  (f): glossy grain with chips, V-shapes, and micro-pits on the protruding parts of the grain; (g):
988  half-matte grain of irregular shape with a fine-pitted texture in the protruding parts of the grain;
989  (h): glossy grain with a conchoidal fracture, V-shapes and fine-pits on the protruding parts of the
990  grain.

991
992

993
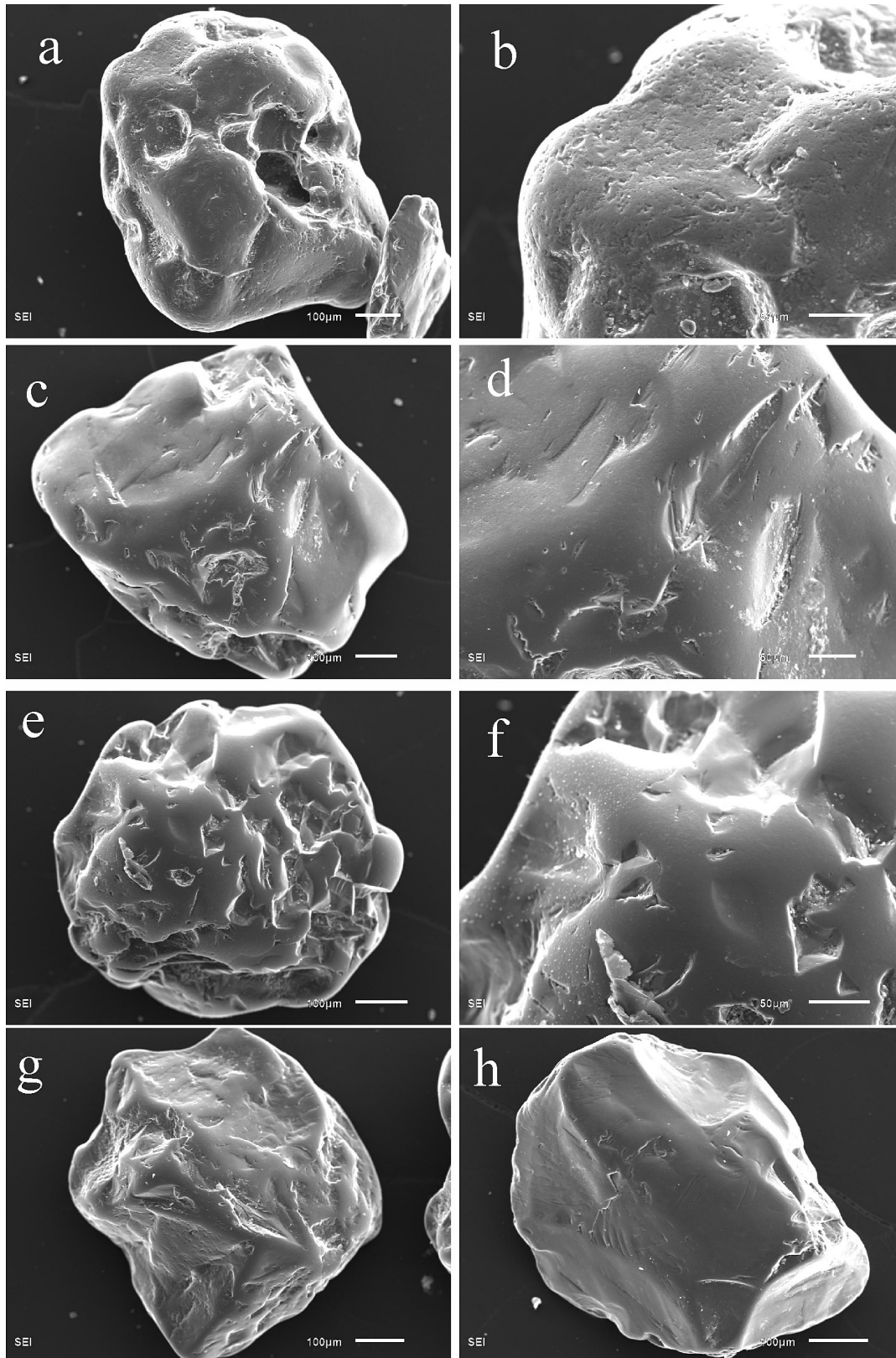
994
995 Annex 12. SEM photos of quartz grains from the section NS-20.
996 (a), (b): matte cavernous grain with a micro-pitted surface and individual crescentic and V-shaped
997 percussions, (c), (d): glossy grain with a smooth surface, grooves, and individual micro-pits, (e),
998 (f): glossy grain with deep groove and single V-shaped percussions, (g): glossy grain of irregular
999 shape with separate V-shaped percussions and a deep-pits, (h): glossy grain with presedimental
1000 conchoidal fractures and scratches.
1001
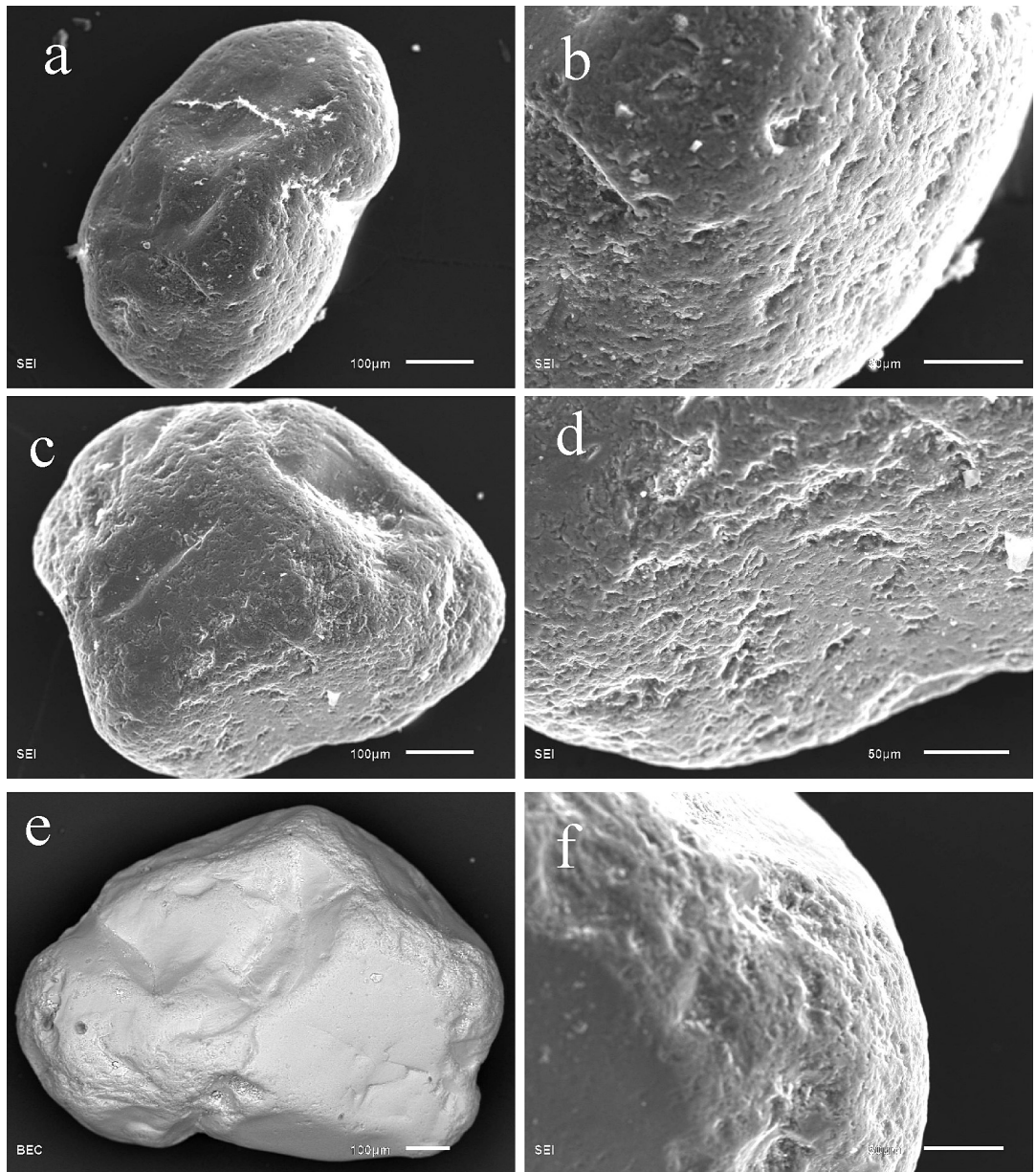
1002
1003     Annex 13. SEM photos of quartz grains from the section NS-22.
1004     (a), (b): glossy grain with a fine-pitted surface, (c), (d): glossy grain with a fine-pitted surface,
1005     (e), (f): glossy grain with fine-pits on the protruding parts of the grain.
1006
1007